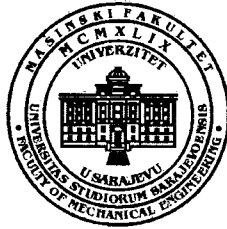


257

UNIVERSITY OF SARAJEVO
FACULTY OF MECHANICAL ENGINEERING



UNIVERZITET U SARAJEVU
MAŠINSKI FAKULTET SARAJEVO

•Wilsonovo šetalište 9, 71 000 Sarajevo, Bosna i Hercegovina, Tel. +387 33 729 800 , Fax.+ 387 33 653 055 •

Broj: 06-VL- 228 /21
Sarajevo, 21.01.2021.

Bosna i Hercegovina
Federacija Bosne i Hercegovine
SARAJEVO

21-01-2021

Opis posla	Redni broj	Broj prijega
Jednica		
01	04	151-31-81

SKUPŠTINA KANTONA SARAJEVO
Elvedin Okerić, Predsjedavajući Skupštine

Predmet: Odgovor na zastupničko pitanje

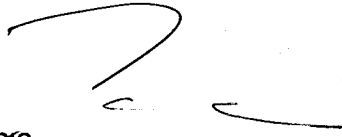
124

Veza: Vaš dopis broj 01-04-151-31/21 od 6.01.2021. godine


Poštovani g. Okerić,

U prilogu se nalazi odgovor na zastupničko pitanje vezano za dosadašnja iskustva mjerenja aerozagađenja u Kantonu Sarajevo.

s poštovanjem,



prof. dr. sc. Zvezdana Hjelonja





•Wilsonovo šetalište 9, 71 000 Sarajevo, Bosna i Hercegovina, Tel. +387 33 729 800, Fax. + 387 33 653 055 •

Odgovor na poslaničko pitanje

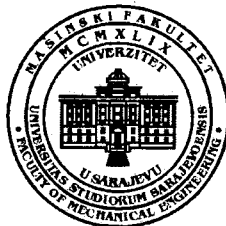
Tekst pitanja: Ljubazno molim da me izvijestite o dosadašnjim iskustvima mjerenja aerozagađenja od strane Mašinskog fakulteta Univerziteta u Sarajevu. Da li imamo neke nove podatke i informacije na osnovu kojih možemo poduzeti konkretne mjere na smanjenju aerozagađenja?

Odgovor

Zahvaljujemo na postavljenom pitanju i prilici koju ste nam dali da Vas izvijestimo o aktivnostima koje se odvijaju na Mašinskom fakultetu Univerziteta u Sarajevu u kontekstu borbe protiv zagađenja zraka. Mašinski fakultet je vodeća visokoškolska ustanova u Bosni i Hercegovini kada su u pitanju napredna istraživanja zagađenosti zraka i ima dugu tradiciju istraživanja ove teme, koja traje preko 50 godina. S obzirom da se pitanje odnosi na nove podatke i informacije, u odgovoru ćemo se fokusirati na najnovije projekte koji su u fazi realizacije, a to su mjerenja i analize temperaturne inverzije, lebdećih čestica, crnog ugljika, ultrafinih čestica (nanočestica) te mjerenja visoke prostorne rezolucije.

Temperaturna inverzija je prirodni fenomen koji je u direktnoj vezi sa prekomjernim zagađenjem zraka u Sarajevu. Uprkos tome što je to već odavno poznata činjenica, nisu postojali ključni podaci o temperaturnoj inverziji koja se pojavljuje iznad Sarajeva. Dva izuzetno sofisticirana projekta su aktivna na Mašinskom fakultetu u okviru kojih se mjeri, analizira i procjenjuje utjecaj temperaturne inverzije:

- 1) mjerenja upotrebom specijalne bespilotne letjelice (drona) koji mjeri vertikalne profile, kako temperature, tako i drugih parametara, kao što su pritisak i vlažnost zraka te koncentracije lebdećih čestica $PM_{1.0}$, $PM_{2.5}$ i $PM_{10.0}$. Tokom prethodne tri godine napravljene su analize za lokaciju Mašinskog fakulteta i općinu Ilijaš, a u ovoj godini se očekuju novi rezultati iz općina Vogošća i Hadžići. Do sada prikupljeni podaci ukazuju na to da su karakteristike inverzionog sloja veoma nepovoljne, te da se isti pojavljuje već pri visinama od 100 metara iznad tla i ima veoma jak gradijent temperature od preko 30 kelvina po kilometru, što pojednostavljeno rečeno znači da se formira „poklopac“ iznad grada. Naročito nepovoljni profili su izmjereni u Ilijašu u januaru 2020.g. Ova istraživanja će se nastaviti i u budućnosti, a osnovni rezultati i zaključci iz dosadašnjih mjerenja su publikovani i dostupni putem linka <https://doi.org/10.2298/TSCI180227250M>
- 2) sistem kontinuiranog mjerenja temperaturne inverzije u realnom vremenu, razvijen na Mašinskom fakultetu, je u saradnji sa JP Sarajevo instaliran na sve stubove trebevičke žičare i putem interneta daje podatke o profilu temperature iznad Sarajeva, a do visine dolazne stanice na Trebeviću (koja se nalazi na 1200 metara nadmorske visine). Ovo je jedan od najmodernijih sistema na svijetu koji u odnosu na mjerenja dronom ima prednost da je stalno aktivan tj. da imamo informaciju o profilu temperature, vlažnosti, vjetrova i lebdećih čestica 24/7. Mašinski fakultet je putem web linka dao na korištenje ove izuzetno dragocjene podatke članovima Stručnog tijela za koordinaciju i nadzor nad primjenom Plana interventnih



•Wilsonovo šetalište 9, 71 000 Sarajevo, Bosna i Hercegovina, Tel. +387 33 729 800 , Fax. + 387 33 653 055 •
mjera u slučajevima prekomjerne zagađenosti zraka u Kantonu Sarajevo da ih koristi u svom radu i ovo je već druga zima da se ovaj alat koristi za tu namjenu.

Lebdeće čestice (eng. *particulate matter*, skraćeno PM) su najvažnija pojedinačna komponenta zagađenja zraka u Sarajevu i zato im je posvećena posebna pažnja. Na Mašinskom fakultetu je razvijena piramidalna shema mjerenja koncentracija PM (frakcije PM₁₀, PM_{2.5} i PM₁) koja uključuje referentnu gravimetrijsku metodu, ekvivalentnu optičku metodu i našu vlastitu metodu zasnovanu na mobilnim senzorima visoke rezolucije. Ova metodologija je u svijetu prepoznata kao optimalna strategija mjerenja jer spaja najbolju tačnost (vrh piramide) sa najnižom cijenom i najboljom rezolucijom (osnovica piramide). Rezultati naših istraživanja su nedavno objavljeni u jednom od najprestižnijih časopisa na svijetu u ovoj oblasti, Atmospheric Measurement Techniques, i javno su dostupni ovdje: <https://doi.org/10.5194/amt-13-6427-2020>

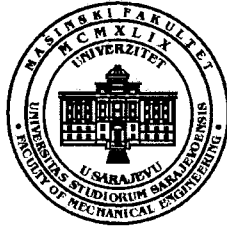
Crni ugljik (eng. *black carbon*, skraćeno BC) nastaje nepotpunim sagorijevanjem fosilnih goriva (drva, ugalj, dizel gorivo itd.) i veoma je važno mjeriti i analizirati njegovu koncentraciju u zraku. S tim u vezi, kontinuirana mjerenja crnog ugljika, kao i analiza svih njegovih karakteristika, se vrše na Mašinskom fakultetu u Sarajevu počev od decembra 2019. godine. Pri tome se koristi najmodernija oprema koja je donirana fakultetu od strane Švedske Ambasade u BiH putem ureda UN-a u BiH. Ministarstvo prostornog uređenja, građenja i zaštite okoliša Kantona Sarajevo je finansiralo nabavku potrošnog materijala i servisiranje opreme, za eksploataciju do 15.6.2021.g. Rezultati ovih mjerenja su pokazali da imamo veoma visoku koncentraciju crnog ugljika u zraku tokom zime i umjerenu koncentraciju tokom ljeta, što je dokaz da je osnovni izvor zagađenja upotreba fosilnih goriva. Detaljnija analiza optičkih karakteristika crnog ugljika je pokazala da je dominantan izvor zagađenja u zimskom periodu loženje drva i uglja, a u ljetnom periodu motorna vozila.

Ultrasitne čestice (nanočestice) predstavljaju najsitnije lebdeće čestice čiji se prečnik mjeri milijarditim dijelovima metra. One su najopasnije po zdravlje ljudi, jer zbog svojih fizikalnih karakteristika mogu da prodru do svih dijelova tijela, pa i do mozga gdje se trajno nakupljaju. Maseni spektrometar nanočestica je u funkciji od decembra 2019.g. zahvaljujući donaciji Švedske Ambasade u BiH, UN-a (putem programa UNDP) i vlastitim naporima Mašinskog fakulteta. Ministarstvo prostornog uređenja, građenja i zaštite okoliša Kantona Sarajevo je finansiralo nabavku potrošnog materijala i servisiranje spektrometra nanočestica do 15.6.2021.g. Rezultati mjerenja su pokazali izuzetno veliki broj nanočestica u zraku, ne samo tokom zimskog, već i tokom ljetnog perioda. Najveći broj nanočestica ima dijametar oko 100 nanometara (što je približno jednako dijametru korona virusa) te se ovaj aparat koristio i za procjenu efikasnosti maski za lice u kontekstu epidemioloških mjera. Osim fosilnih goriva, postoje i drugi izvori nanočestica kao što su frikcioni elementi kočnica automobila i taj doprinos tek treba istražiti u budućnosti.

ZAKLJUČAK

Mjerenja na Mašinskom fakultetu u Sarajevu po svojoj metodologiji, korištenoj opremi i načinu analize podataka spadaju u red najmodernijih svjetskih projekata u ovoj oblasti. Ona su pokazala da je glavni uzrok zagađenja zraka intenzivna upotreba fosilnih goriva u kombinaciji s nepovoljnom klimom (temperaturna inverzija). Takođe su utvrđene visoke koncentracije crnog ugljika i nanočestica, što sveobuhvatno predstavlja veliku opasnost po zdravlje

UNIVERSITY OF SARAJEVO
FACULTY OF MECHANICAL ENGINEERING



UNIVERZITET U SARAJEVU
MAŠINSKI FAKULTET SARAJEVO

•Vilsonovo šetalište 9, 71 000 Sarajevo, Bosna i Hercegovina, Tel. +387 33 729 800 , Fax. + 387 33 653 055 •
stanovnika, naročito u zimskom periodu. Problem se može ublažiti ograničenjem loženja uglja i drva i smanjivanjem broja vozila sa neodgovarajućim ekološkim karakteristikama, ali će potpuno rješenje problema biti moguće tek kada se završi proces dekarbonizacije. Mašinski fakultet će i u narednom periodu svoje resurse koristiti za istraživanja ovog problema. Takođe Vas želimo pozvati da posjetite Mašinski fakultet u Sarajevu i laboratorije u kojima se vrše ova važna istraživanja.

Izveštaj pripremio: prof. dr. Adnan Mašić

• ID: 4200415950008; PDV: 4200415950008 •

www.mef.unsa.ba

EXPERIMENTAL STUDY OF TEMPERATURE INVERSIONS ABOVE URBAN AREA USING UNMANNED AERIAL VEHICLE

by

**Adnan MAŠIĆ*, Dževad BIBIĆ, Boran PIKULA, Emina DŽAFEROVIĆ-MAŠIĆ,
and Rajfa MUSEMIĆ**

Faculty of Mechanical Engineering, University of Sarajevo, Sarajevo, Bosnia and Herzegovina

Original scientific paper
<https://doi.org/10.2298/TSCI180227250M>

Vertical temperature profiles represent a very important factor for various analytical and numerical studies, such as weather forecasts, air pollution models and CFD simulations. These temperature profiles are especially important during the winter periods, when temperature inversions occur. The cities in the natural valleys, such as the city of Sarajevo, B&H, are strongly affected by this phenomenon. In this paper, a method for quantitative characterization of vertical temperature profiles, which is based on the in-house developed data acquisition system and the unmanned aerial vehicle, is presented. Comprehensive calibration and verification procedure was performed and explained in details. Field measurements were focused on the winter period and extreme temperature inversion scenarios. The correlation with the air pollution in the city, for the same period, was discussed as well.

Key words: *temperature inversion, unmanned aerial vehicle, data acquisition system, air pollution, Sarajevo*

Introduction

Temperature inversion is a natural phenomenon which occurs often in the winter period: layer of air where temperature increases with height is formed at some altitude above the ground. Natural convection is prevented through the inversion layer, which acts as the lid above the area. If the temperature inversion appears above the urban area, it is usually associated with increased air pollution below the inversion layer. The temperature inversion may last for few hours or sometimes much longer. The height above the ground where inversion layer starts and temperature gradient within inversion layer are two primary quantitative characteristics of the temperature inversion. These quantitative characteristics are important due to several reasons:

- strong inversions appear over cities in the natural valleys, which lead to the dramatic increase of air pollution in such cities,
- reliable data for vertical temperature profiles can be used to predict expected episodes of strong air pollution before pollutants concentrations reach extreme values, and
- vertical temperature profiles are required input for computer programs with models of air dispersion, and simulations in the framework of CFD.

The city of Sarajevo is situated in the natural valley, with relatively harsh climate during the winter. Prior to this study, there were no data available about temperature profiles in

* Corresponding author, e-mail: masic@mef.unsa.ba

typical winter scenarios in Sarajevo. The governmental institutions do not perform measurements of vertical profiles in our country, due to high costs (of traditional methods). The aim of this study is twofold:

- to obtain reliable data for vertical temperature profiles above the city of Sarajevo and
- to demonstrate and evaluate a novel, innovative, approach for low-cost vertical sampling which is accurate and reliable.

Several techniques were considered. The weather balloon with radiosonde was obvious candidate, but due to some limitations [1] and associated costs – it was rejected. An interesting possibility was to use the instrument which measures the microwave radiation at different elevation angles [2], but it was not available and the accuracy of such approach was questionable. The decent option is the network of ground-based automatic weather stations, such as the one presented in [3]. However, it requires significant construction work to build such a network and, strictly speaking, it does not provide vertical profiles, since the individual stations are horizontally displaced (an assumption that the field temperature is horizontally homogeneous in winter period is used). Alternatively, the ropeway could be used for in-situ measurements [4] (there is the same problem with the assumption of horizontal homogeneity of the temperature field). Comprehensive studies that use satellite sensing in combination with numerical simulations [5] and ground-based observations [6] recently appeared.

Finally, the method based on the unmanned aerial vehicle (UAV) was chosen, due to several advantages:

- lower costs (contrary to the weather balloon, UAV can be used many times, making the total cost per single measurement much lower),
- deployment possible anywhere (required landing area is comparable to the car's parking place),
- great vertical alignment and ability to control all flight parameters (including autonomous and repeatable flight paths), and
- possibility to measure the temperature profile in both directions (ascending and descending), *etc.*

The project started in 2014, with the initial evaluation of the concept and first prototype of both data acquisition system (DAS) and small UAV with four motors, taking off for the first time in early 2015 [7]. Various sensors and flight parameters were tested. Evaluation of the prototypes resulted in the decision that all systems should be developed in-house if possible, and for those components where this is not the case (flight controller for example) open-source solutions are preferred over the commercial (closed-source) products. In that way, full control of all DAS and UAV parameters is available at all times.

In the meantime, some other groups reported their attempts to use UAV for measurements of: environmental variables in greenhouses [8], air pollution [9], meteorological variables and methane [10], and air sampling on Ascension Island [11]. Fixed-wing, commercially available UAV and sensors were used to measure vertical temperature profiles in [12, 13]. These are not suitable for urban environment (aircrafts require space for landing) and do not perform vertical flights.

The apparatus

Main components of our system are DAS and UAV. The simplified schematics of the DAS is presented in the fig. 1. The temperature sensing element is a thermistor with the negative temperature coefficient (NTC). It has the small thermal capacity (thus, fast response to the changes of ambient temperature), small dimensions (0.8 mm in diameter) and very good mechanical properties (it is encapsulated in glass).

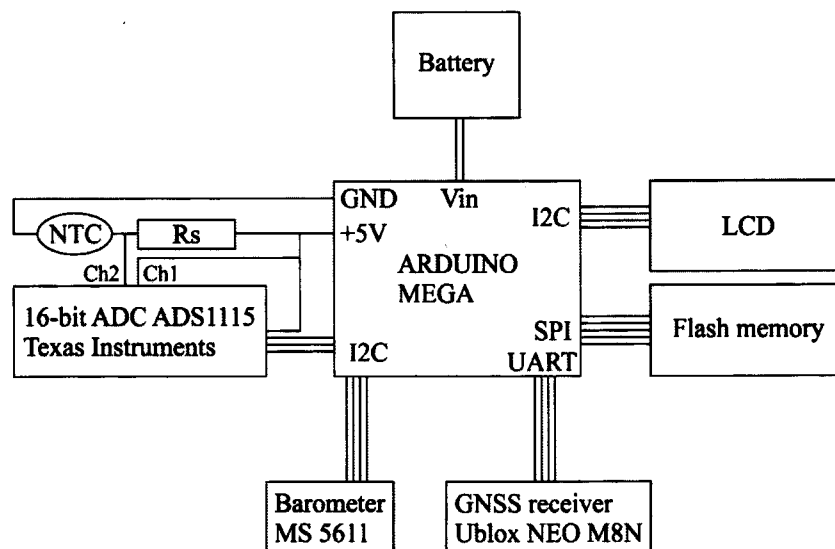


Figure 1. Simplified block-diagram of the DAS

The reference voltage of 5 V was applied to the NTC over the serial resistor, R_s , which was chosen in such a way that the self-heating effect was eliminated (an order of magnitude below the sensor's uncertainty). Analog to digital converter (ADC) is Texas Instruments ADS1115 (16-bit), which offers 0.1875 mV resolution in the interval from -6.144 V to $+6.144$ V. Two channels (out of four) of ADS1115 are used for temperature readings: one permanently monitors the 5 V voltage reference, the other samples the voltage across the NTC (as shown in the fig. 1). The ADC has I2C bus interface, and an Arduino Mega was used as the host microcontroller. Apart from temperature, the DAS is equipped with GNSS receiver (Ublox 8th generation, with the concurrent reception of signals from GPS and GLONASS satellites), barometer, LCD display and card memory slot. Regarding the interfaces, the LCD and barometer are I2C devices, the flash memory interface is SPI, while the GNSS receiver sends NMEA (National Marine Electronics Association) sentences over the serial interface.

The UAV has evolved dramatically from the first prototype described in [7]. Now it has six motors on the frame which is our modification of commercially available carbon fiber frame. CAD model was created in SolidWorks®, and various parameters were modified and optimized in this process. Finally, the wheelbase of 710 mm was chosen (fig. 2 shows the actual frame, its CAD model and mounted DAS). The propulsion system is commercially available DJI E800, the

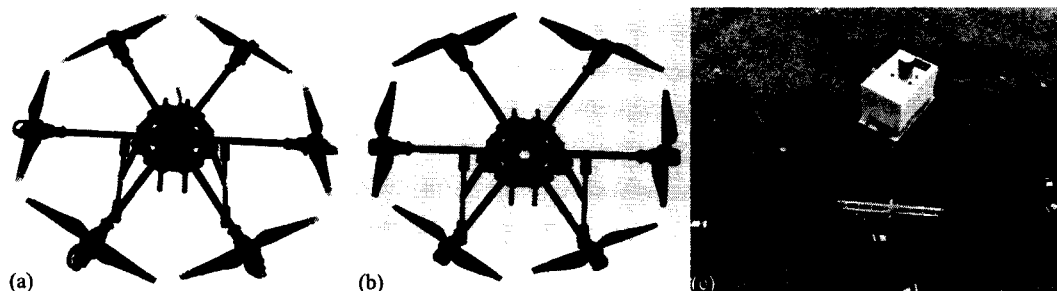


Figure 2. Hexacopter chassis (a), its CAD model (b) and the DAS atop (c)

flight controller is open-source Pixhawk with Arducopter software and many smaller parts are designed in-house and printed on a 3-D printer. Radio control system works in 433 MHz bands. There is also a video downlink which streams the video from two onboard cameras.

Calibration and verification

For highly accurate and reliable measurements of temperature using thermistors, it is necessary to perform the calibration of the thermistor. We have addressed this step very carefully. The calibration of the thermistor was performed at the Institute of Metrology of Bosnia and Herzegovina, using the following cutting-edge equipment, fig. 3:

- Isotech parallel tube liquid bath 915.
- Isotech 670SQ SPRT temperature sensor.
- Isotech F900 precision thermometry bridge.
- Tektronix Keithley 2000 digital multimeter.

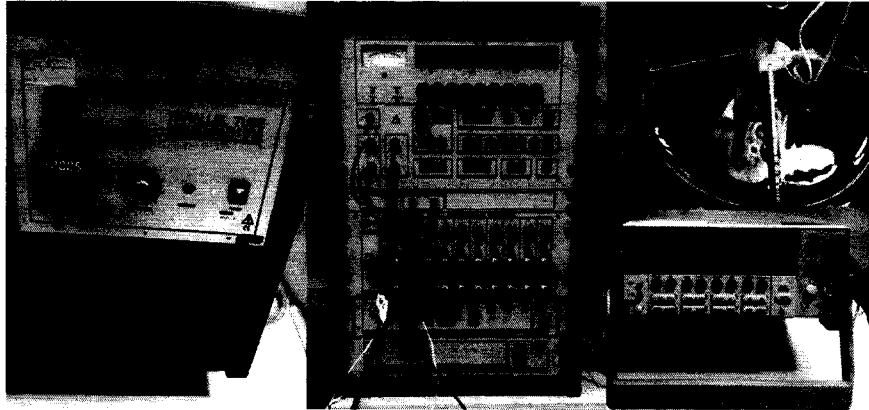


Figure 3. The equipment used for the calibration of the thermistor

The calibration interval was from $-20\text{ }^{\circ}\text{C}$ to $+40\text{ }^{\circ}\text{C}$, with six calibration points: -20 , -10 , 0 , 10 , 25 , and $40\text{ }^{\circ}\text{C}$. The uncertainty of the reference thermometer was only 2 mK , and taking into account all the factors (reference thermometer, bath, bridge, unit under test, self-heating, hysteresis and repeatability), the total uncertainty of this calibration procedure is estimated to be below 20 mK in the entire interval (that is a conservative estimate). The thermistor's calibration points were shown in the fig. 4, together with the chosen interpolation method, the Steinhart-Hart equation [14]:

$$\frac{1}{T} = a + b \ln(R) + c \ln(R)^3 \quad (1)$$

The coefficients a , b , and c were calculated using the least squares regression. We can see from fig. 4 that the state of the art technology used in the calibration process, translated into a perfect fit on the graph. Of course, the right choice of the analytical curve is important as well, and the Steinhart-Hart eq. (1) is well known and recommended interpolation curve for the NTC thermistors. This is a very important step, since the NTC thermistor has non-linear characteristic (which is clearly illustrated in fig. 4). The non-linear nature of NTC curve can be represented analytically, if we calculate the first derivation of temperature in eq. (1):

$$\frac{dT}{dR} = -\frac{b + 3c \ln(R)^2}{R [a + b \ln(R) + c \ln(R)^3]^2} \quad (2)$$

Alternatively, the polynomial fit of the fifth order could be used as well, or similar approach proposed in [15].

Together with the NTC thermistor, we have calibrated the serial resistor, R_s , as well. Its temperature dependence in the selected interval is linear, and the value of its resistance changed no more than 6.8% when going from $-20\text{ }^\circ\text{C}$ to $+40\text{ }^\circ\text{C}$.

After the calibration in the laboratory, the DAS was mounted on the UAV. Computational fluid dynamics simulations, such as [8], clearly show that the optimal position of the DAS is above the rotors, where the air speed is much smaller (than below the rotors). Despite the fact that our DAS was mounted in an optimal position (considering the technical limitations), another experiment was performed: second DAS was prepared and tied to the UAV with 20 m long thread. The aim of the experiment was to check if there is any significant influence of the propellers on measured values of temperature. The thread length of 20 m was long enough to keep the bottom DAS free of turbulence created by propellers (we have verified that experimentally). At the same time, the chosen length didn't induce any significant difference of temperatures between two sensors (under test conditions, 20 m difference in height corresponds to $0.1\text{ }^\circ\text{C}$ difference in temperature). Thus, two sensors are expected to produce a very good agreement.

The typical vertical mission was executed, with maximum altitude (of UAV and top DAS) of 520 m above the ground level (AGL). The results of the experiment are shown in fig. 5. We can see from the graph in fig. 5 that two sensors show very similar results, which means that the influence of the rotors on the primary DAS is not significant.

Finally, despite the fact that the thermistor quickly reacts to the changes of ambient temperature, its time constant cannot be neglected. The UAV typically flies with vertical speed 2-3 m/s, and some hysteresis is expected, if we measure the temperature in both directions (ascending and descending). Figure 6 shows the hysteresis during the typical flight. This effect cannot be avoided, but there is an excellent opportunity for correction when using UAV: both the ascending, T_A , and descending, T_D , temperature can be used, and the arithmetic mean, T_{AVG} , is calculated, for each altitude point:

$$T_{AVG} = \frac{T_A + T_D}{2} \quad (2)$$

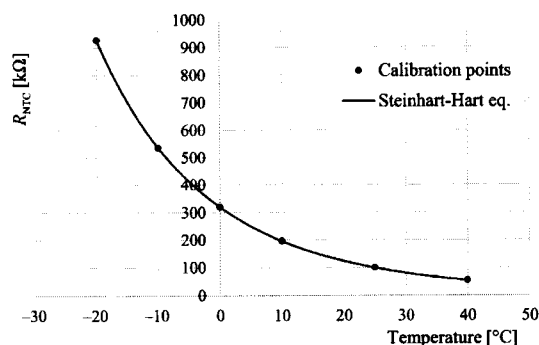


Figure 4. Calibration points and the interpolation curve

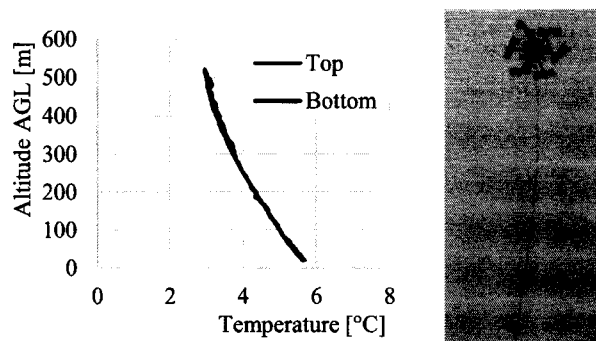


Figure 5. Test of the influence of propellers

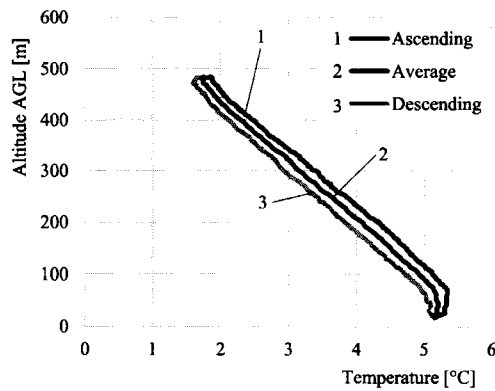


Figure 6. Continuous temperature measurement with UAV during the ascending and descending phase of flight

altitude, the greatest contribution comes from the possibility that local air pressure changes during the flight, which leads to the incorrect calculation of altitude. However, typical flight time is only about 10 minutes, and it is very unlikely that the local air pressure is going to change dramatically during such a short time interval. In reality, no altitude drifts greater than 10 m were ever observed during this research. Altitude is measured using GNSS as well, but GNSS is relatively accurate for determination of horizontal position, which is not the case for the vertical position. Thus, the barometer is used for altitude calculations, with great accuracy and stability.

Results and discussion

A field campaign was performed in Sarajevo, during the winter 2016/2017, at location $43^{\circ}53'37''\text{N}$, $18^{\circ}22'31''\text{E}$ with an elevation of 557 m above sea level (denoted as L1 on pictures). Both ascending speed and descending speed are indicated in every figure. Local time and date were stamped as well. We will present 18 characteristic temperature profiles, which cover all scenarios that we have observed during the campaign. Flights are performed up to 1 km above ground level (1.5 km above sea level). Ambient temperatures occasionally went below -20°C . Figure 7 illustrates the typical view from the UAV.

An overview of all flights is given in the tab. 1.

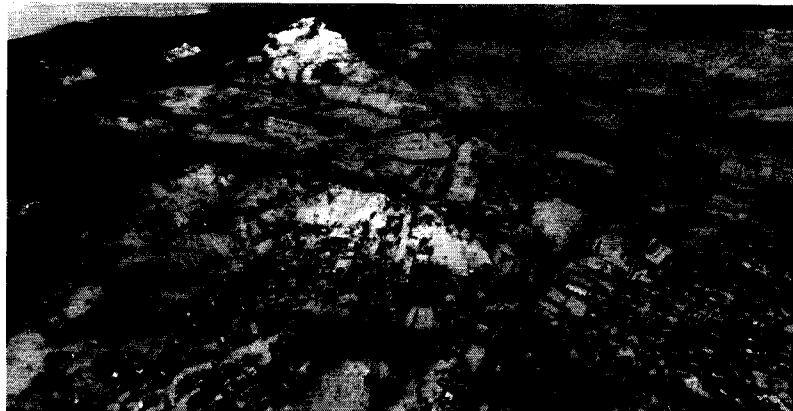


Figure 7. View from the UAV's main camera during the measurement

The graph in fig. 6 shows this correction: the temperature is measured continuously during the ascending and the descending phase of the flight, and the eq. (2) is used to estimate actual temperature. This methodology is applied to all measurements in this study.

Taking into account results of the calibration (uncertainty below 0.02°C), test of rotor's influence (estimated below 0.20°C) and the uncertainty due to the thermal time constant of the sensor (estimated below 0.25°C), we can claim that all results in this study have the uncertainty of 0.5°C or less.

The altitude AGL was calculated from the barometric formula; barometer was used for measurements of air pressure (temperature correction was implemented). Regarding the uncertainty of

Table 1. Summary of all measurements

No.	Flight time	Observed temperature profile
1	25.12.2016, 11:40	Very strong inversion starts from 156 m AGL
2	25.12.2016, 14:40	Very strong inversion starts from 118 m AGL
3	26.12.2016, 10:20	Very strong inversion starts from 126 m AGL
4	27.12.2016, 15:20	No inversion observed
5	07.01.2017, 09:50	No inversion observed
6	11.01.2017, 11:00	No inversion observed
7	12.01.2017, 16:30	Inversion develops before sunset
8	15.01.2017, 11:40	Strong inversion layer starts from 390 m AGL
9	15.01.2017, 16:10	No inversion observed
10	22.01.2017, 10:20	Strong inversion layer starts from 316 m AGL
11	24.01.2017, 09:20	Strong inversion layer starts from 132 m AGL
12	25.01.2017, 08:20	No inversion observed
13	28.01.2017, 10:40	Mild inversion starts from 113 m AGL
14	29.01.2017, 10:20	Strong inversion starts from 47 m AGL
15	29.01.2017, 16:30	Inversion develops before sunset, mild inversion layer starts from 424 m AGL
16	31.01.2017, 17:20	Inversion develops before sunset
17	12.02.2017, 09:30	Strong inversion starts at 612 m AGL
18	15.02.2017, 11:30	Strong inversion starts from 469 m AGL

Graphs 1-3 (as described in tab. 1) show strong temperature inversions which are formed very close to the ground (the worst combination); the inversion layer starts at about 150 m above the ground and has temperature gradients in the inversion layer up to 33.5 K/km (on graph 1). This is very strong temperature inversion, and it has dramatic effects; inversions with gradients stronger than 5 K/km are known to produce severe effects on local air pollution [3]. Graphs 4-6 occasionally show very cold air, but without temperature inversion. In fig. 9, we have different scenarios. Graph 7 shows the development of inversion before sunset (due to the cold ground), with no temperature inversion in the air above 100 m AGL. Graphs 8 and 10 show temperature inversion with an interesting 'Z' profile (such profiles are discussed in [16]): inversion exists higher above the ground, and the temperature gradient is typically between 5 and 10 K/km in the inversion layer. Graphs 9 and 12 do not show inversion, while Graph 11 indicates low inversion layer height (132 m) with the gradient of about 7.9 K/km. Graphs 13-15 again show low inversion layer height with different gradients: 4.9, 10.9, and 0.2 K/km. There is again the effect of the cold ground with no inversion above 100 m AGL in Graph 16, while Graphs 17 and 18 show strong inversions that are formed higher (500 m or more) above the ground.

Figure 11 shows daily average concentrations of PM10 (particulate matter, particles smaller than 10 mm in diameter) suspended in the air, measured by the nearest governmental monitor, the Federal Hydrometeorological Institute B&H. The PM10 concentrations were measured by the beta-attenuation monitor Verewa F701 at Bjelave, Sarajevo, some 4.7 km from L1. On the secondary y-axis we have plotted reciprocal value of the inversion layer height, $1/h$ for all 18 available measurements, tab. 1. Points where inversion layer is close to the ground are appearing high on the secondary y-axis, while points without inversion sit on the horizontal axis ($1/h = 0$ for such points). From fig. 11, we can clearly see the correlation between excessive air pollution and strong temperature inversion: whenever inversion layer exists at low altitudes above the ground, high PM10 concentrations are recorded. Furthermore, when the inversion in the boundary layer breaks up, PM10 concentrations drop significantly. Some observed values

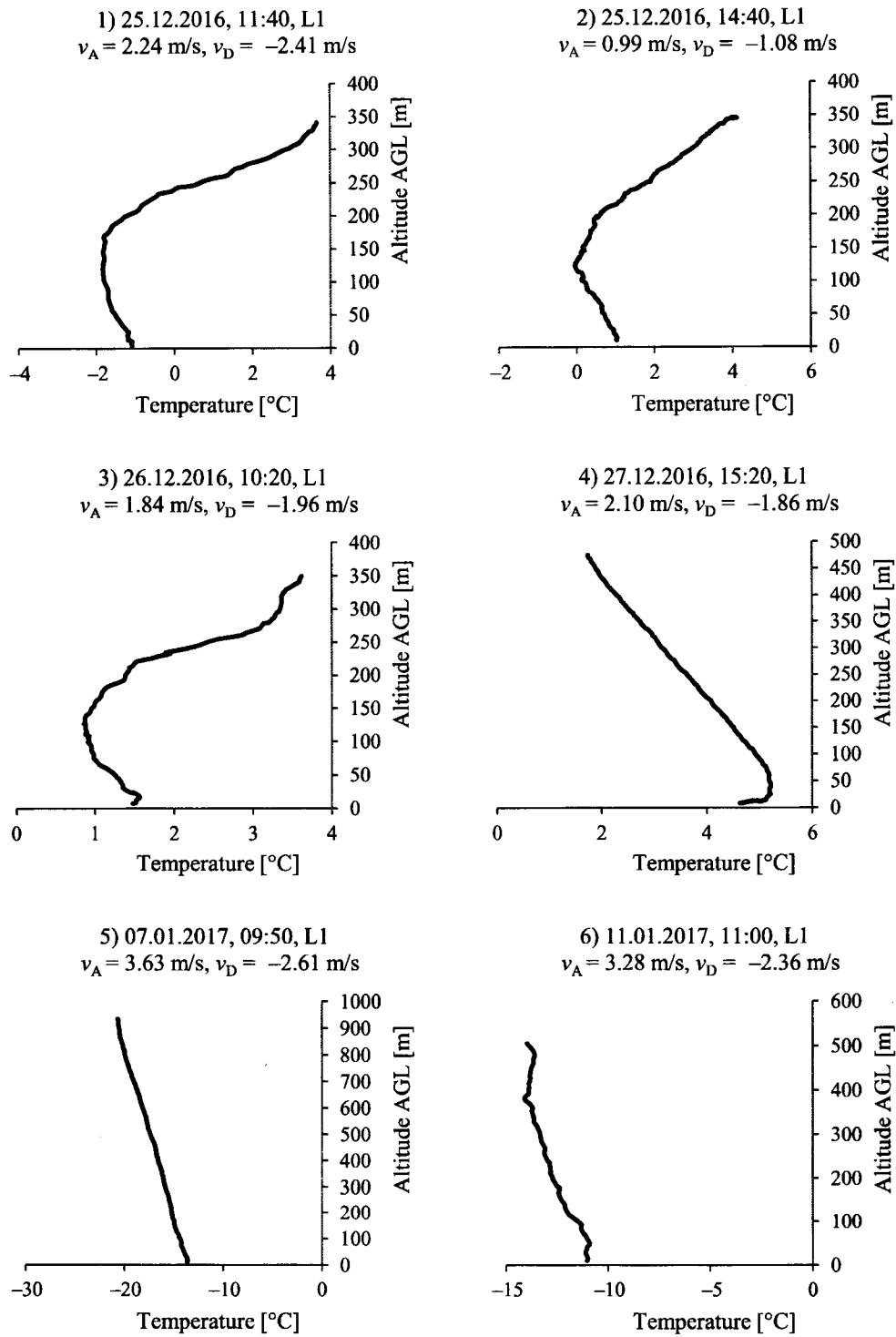


Figure 8. Temperature profiles

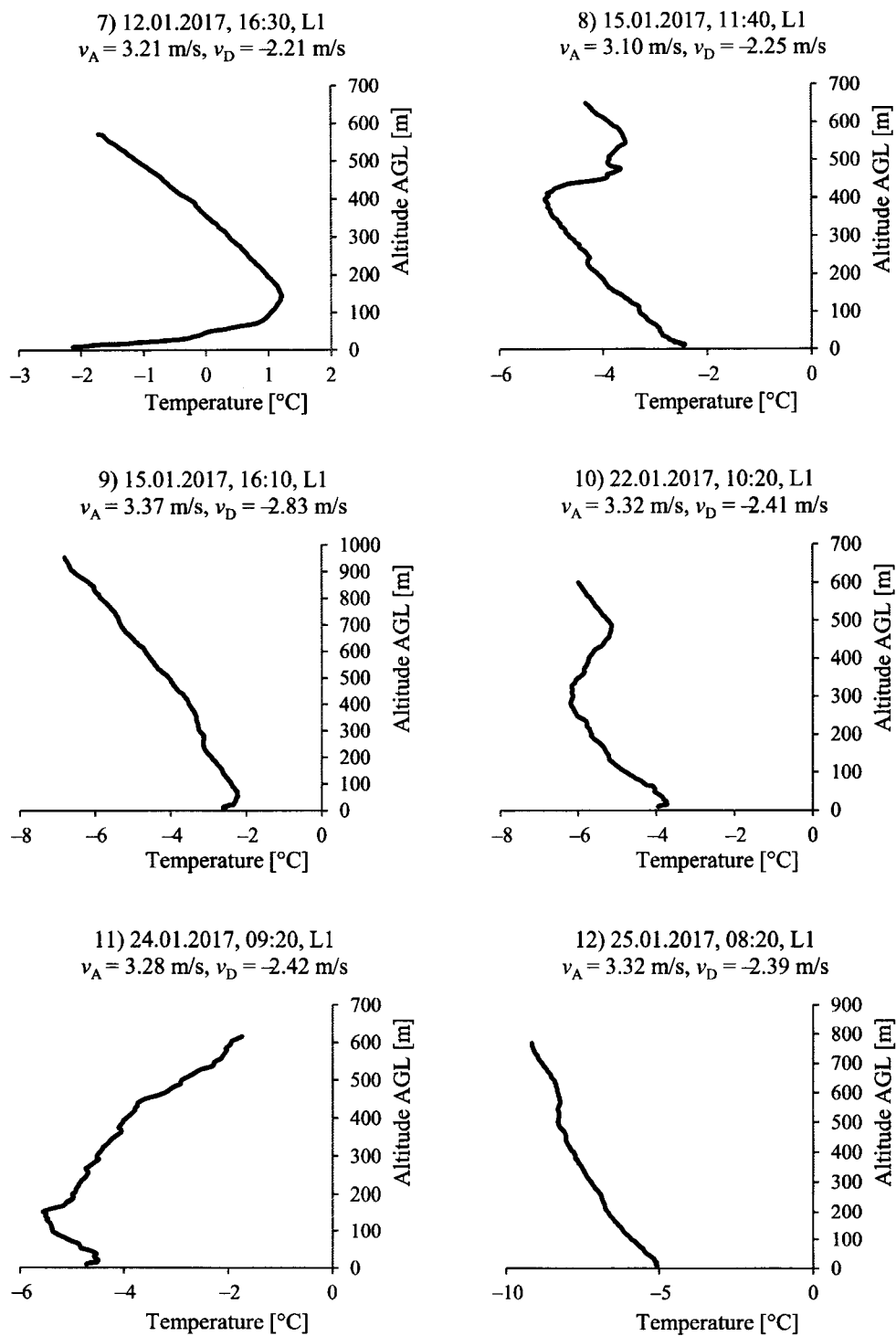


Figure 9. Temperature profiles

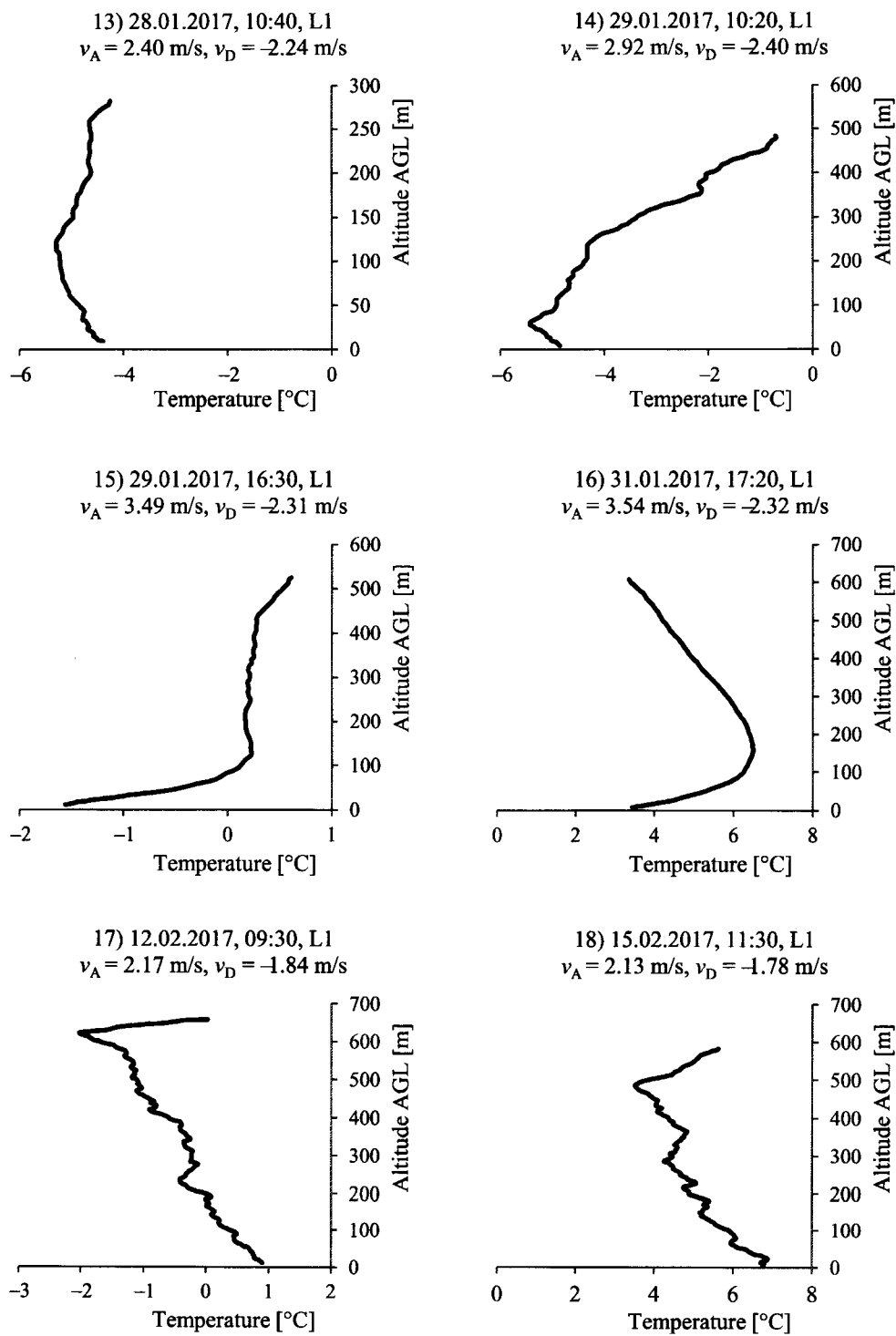


Figure 10. Temperature profiles

of PM10 concentrations (up to 600 mg/m^3) are 12 times greater than limit of 50 mg/m^3 , recommended by the World Health Organization and adopted from many governmental institutions. Such level of air pollution represents major risk for the health of humans.

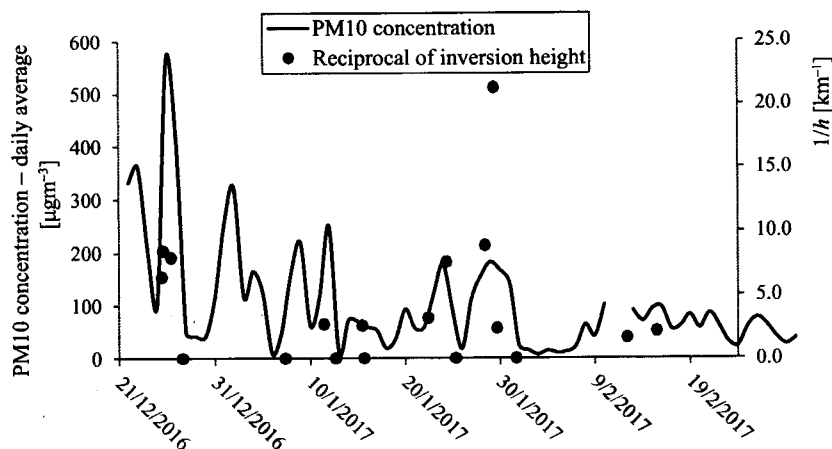


Figure 11. Correlation of PM10 air pollution and (reciprocal value of) inversion layer height

Conclusions

A comprehensive method for measurements of vertical temperature profiles using unmanned aerial vehicles is developed. Calibration and validation of all elements and procedures used for measurements were performed with great attention to all possible sources of uncertainties. A field campaign was organized during the winter 2016/2017 in Sarajevo. Various scenarios of temperature inversions were measured and analyzed. The collected data indicate unfavorable conditions: the temperature inversions were strong and shallow; with gradients in the inversion layer exceeding 30 K/km , and inversion layers often appearing below 150 m AGL. Episodes of strong and shallow inversion are correlated with hazardous air pollution, especially PM10 concentrations.

As a suggestion for future work, we propose more measurements during the longer periods. We will try to integrate sensors for air pollution parameters into our system and perform combined measurements of temperature profiles with profiles of various air pollutant concentrations. This will be reported in the near future, hopefully.

Acknowledgment

This work was supported by the Ministry of Education of Canton Sarajevo, No. 11-05-38-16631-8/16.

Also, it would not be at its greatest value without a considerable help of the Institute of Metrology of Bosnia and Herzegovina (IMB&H) and their excellent staff at the Laboratory for Temperature and Humidity, where the calibration of our temperature sensor was performed with the highest quality and international reference and traceability.

Nomenclature

a – coefficient of the first term in
Steinhart-Hart equation

b – coefficient of the second term in
Steinhart-Hart equation

c – coefficient of the third term in Steinhart-Hart equation	T_D – temperature readings during the descend of the UAV, [K]
R – electric resistance, [W]	v_A – vertical velocity of the UAV during the ascend, [ms ⁻¹]
T – temperature, [K]	v_D – vertical velocity of the UAV during the descend, [ms ⁻¹]
T_A – temperature readings during the ascend of the UAV, [K]	

References

- [1] Mahesh, A., et al., Radiosonde Temperature Measurements in Strong Inversions: Correction for Thermal Lag Based on an Experiment at the South Pole, *Journal of Atmospheric and Oceanic Technology*, 14 (1997), Feb., pp. 45-53
- [2] Wolf, T., et al., Analysis of the Vertical Temperature Structure in the Bergen Valley, Norway, and its Connection to Pollution Episodes, *Journal of Geophysical Research: Atmospheres*, 119 (2014), 18, pp. 10645-10662
- [3] Largeron, Y., Staquet C., Persistent Inversion Dynamics and Wintertime PM10 Air Pollution in Alpine Valleys, *Atmospheric Environment*, 135 (2016), June, pp. 92-108
- [4] Zawadzka, O., et al., Study of the Vertical Variability of Aerosol Properties Based on Cable Cars in-Situ Measurements, *Atmospheric Pollution Research*, 8 (2017), 5, pp. 968-978
- [5] Wang, Q., et al., A Quantitatively Operational Judging Method for the Process of Large Regional Heavy Haze Event Based on Satellite Remote Sensing and Numerical Simulations, *Atmosphere*, 8 (2017), 11, pp. 1-15
- [6] Liu, B., et al., Study of Continuous Air Pollution in Winter Over Wuhan Based on Ground-Based and Satellite Observations, *Atmospheric Pollution Research*, 9 (2018), 1, pp. 156-165
- [7] Masic, A., Unmanned Aerial Vehicle as Data Acquisition System, *Journal of Trends in the Development of Machinery and Associated Technology*, 1 (2015), Jan., pp. 181-184
- [8] Roldan, J. J., et al., Mini-UAV Based Sensory System for Measuring Environmental Variables in Greenhouses, *Sensors*, 15 (2015), 2, pp. 3334-3350
- [9] Villa, T. F., et al., Development and Validation of a UAV Based System for Air Pollution Measurements, *Sensors*, 16 (2016), 12, pp. 1-15
- [10] Brosy, C., et al., Simultaneous Multicopter-based Air Sampling and Sensing of Meteorological Variables, *Atmospheric Measurement Techniques*, 10 (2017), 8, pp. 2773-2784
- [11] Greatwood, C., et al., Atmospheric Sampling on Ascension Island Using Multirotor UAVs, *Sensors*, 17 (2017), 6, pp. 1-24
- [12] Cassano, J. J., Observations of Atmospheric Boundary Layer Temperature Profiles with a Small Unmanned Aerial Vehicle, *Antarctic Science*, 26 (2014), 2, pp. 205-213
- [13] Dias, N. L., Obtaining Potential Virtual Temperature Profiles, Entrainment Fluxes, and Spectra from Mini Unmanned Aerial Vehicle Data, *Boundary-Layer Meteorology*, 145 (2012), 1, pp. 93-111
- [14] Steinhart, J. S., Hart, S. R., Calibration Curves for Thermistors, *Deep-Sea Research and Oceanographic Abstracts*, 15 (1968), 4, pp. 497-503
- [15] Ilic, D., et al., Temperature Measurements by Means of NTC Resistors and a Two-parameter Approximation Curve, *Measurement*, 41 (2008), 3, pp. 294-299
- [16] Fochesatto, G. J., Methodology for Determining Multilayered Temperature Inversions, *Atmospheric Measurement Techniques*, 8 (2015), May, pp. 2051-2060

Evaluation of optical particulate matter sensors under realistic conditions of strong and mild urban pollution

Adnan Masic¹, Dzevad Bibic¹, Boran Pikula¹, Almir Blazevic¹, Jasna Huremovic², and Sabina Zero²

¹Faculty of Mechanical Engineering, University of Sarajevo, 71000 Sarajevo, Bosnia-Herzegovina

²Faculty of Science, University of Sarajevo, 71000 Sarajevo, Bosnia-Herzegovina

Correspondence: Adnan Masic (masic@mef.unsa.ba)

Received: 16 June 2020 – Discussion started: 8 July 2020

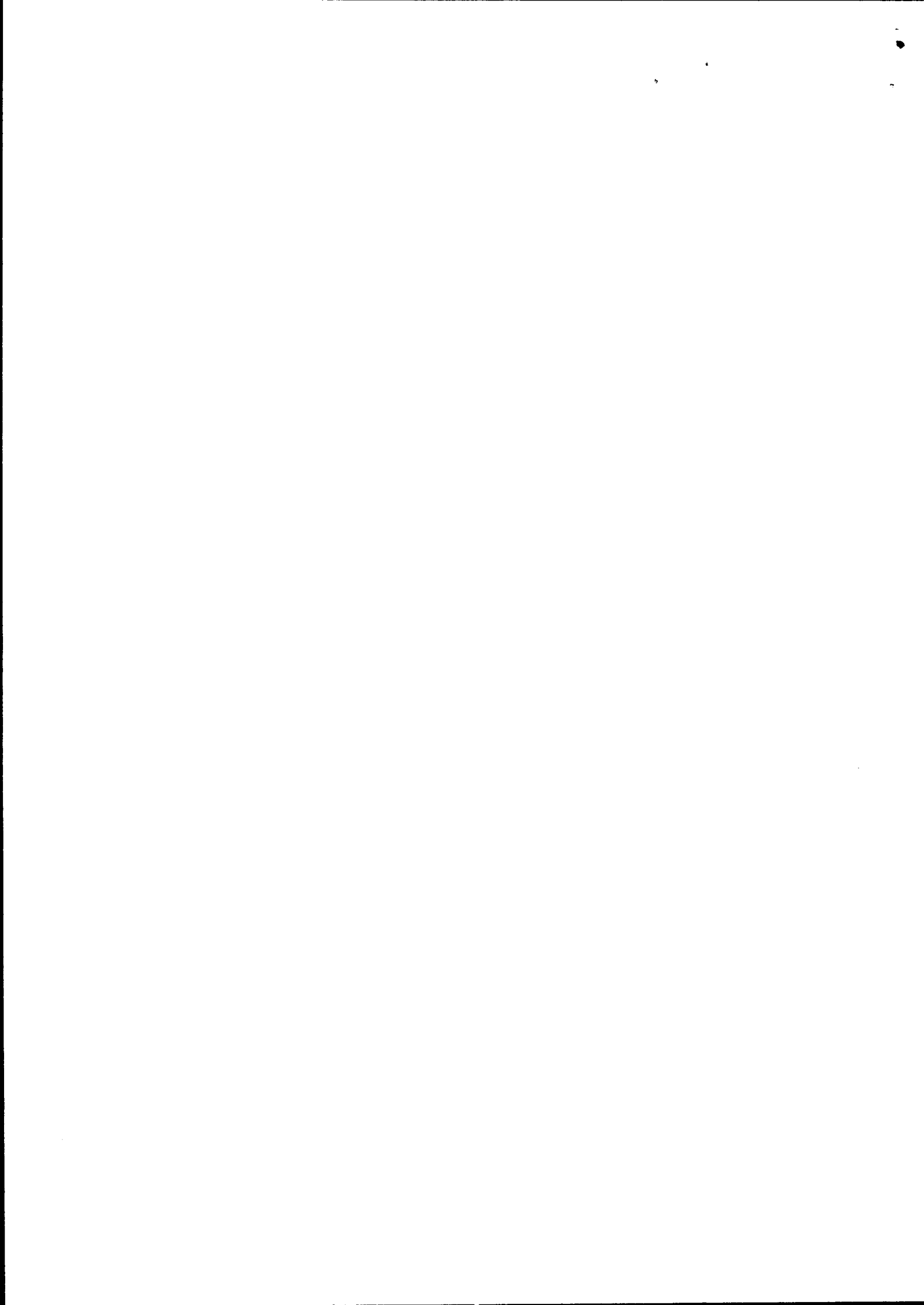
Revised: 20 October 2020 – Accepted: 21 October 2020 – Published: 30 November 2020

Abstract. In this paper we evaluate characteristics of three optical particulate matter sensors/sizers (OPS): high-end spectrometer 11-D (Grimm, Germany), low-cost sensor OPC-N2 (Alphasense, United Kingdom) and in-house developed MAQS (Mobile Air Quality System), which is based on another low-cost sensor – PMS5003 (Plantower, China), under realistic conditions of strong and mild urban pollution. Results were compared against a reference gravimetric system, based on a Gemini (Dadolab, Italy), 2.3 m³ h⁻¹ air sampler, with two channels (simultaneously measuring PM_{2.5} and PM₁₀ concentrations). The measurements were performed in Sarajevo, the capital of Bosnia-Herzegovina, from December 2019 until May 2020. This interval is divided into period 1 – strong pollution – and period 2 – mild pollution. The city of Sarajevo is one of the most polluted cities in Europe in terms of particulate matter: the average concentration of PM_{2.5} during the period 1 was 83 µg m⁻³, with daily average values exceeding 500 µg m⁻³. During period 2, the average concentration of PM_{2.5} was 20 µg m⁻³. These conditions represent a good opportunity to test optical devices against the reference instrument in a wide range of ambient particulate matter (PM) concentrations. The effect of an in-house developed diffusion dryer for 11-D is discussed as well. In order to analyse the mass distribution of particles, a scanning mobility particle sizer (SMPS), which together with the 11-D spectrometer gives the full spectrum from nanoparticles of diameter 10 nm to coarse particles of diameter 35 µm, was used. All tested devices showed excellent correlation with the reference instrument in period 1, with *R*² values between 0.90 and 0.99 for daily average PM concentrations. However, in period 2, where the range of concentrations was much narrower, *R*² values decreased signif-

icantly, to values from 0.28 to 0.92. We have also included results of a 13.5-month long-term comparison of our MAQS sensor with a nearby beta attenuation monitor (BAM) 1020 (Met One Instruments, USA) operated by the United States Environmental Protection Agency (US EPA), which showed similar correlation and no observable change in performance over time.

1 Introduction

Analysis of particulate matter represents a key element for studies of air pollution. Various studies shed light on their effect on health (Downward et al., 2018) and climate (Zhao et al., 2019). In many cases particulate matter is a dominant pollutant among other components of pollution. Therefore, developing a strategy for reliable quantification of particulate matter in ambient air is necessary. The traditional and most accurate approach to measuring the particulate matter concentration in the air is the reference method, based on gravimetric measurements, after the collection of particulate matter by air samplers. The typical time resolution of such measurements is 24 h. Although there are portable air samplers, these measurements are usually performed at fixed locations, such as research supersites. Reference systems are expensive and require a lot of laboratory work. Results are not immediately available because of the time-consuming process of filter treatment. Taking that into account, various governmental institutions usually opt for more affordable and easier-to-use and -maintain equivalent methods. These are usually fixed, semi-automatic stations equipped with beta attenuation monitors (BAMs). The typical time resolution of such sta-



tions is 1 h. If maintained and calibrated properly, the equivalent methods should achieve an acceptable level of agreement with the reference. For example, one long-term comprehensive study (Hafkenscheid and Vonk, 2014) performed at 14 different locations across the Netherlands showed that a linear correction $y = 0.91x - 1.6$, applied to raw readings from BAM, was necessary to achieve the requirements of the Guide to the Demonstration of Equivalence (ECWG, 2010).

Newer methods, based on optical particle sensors (OPS), are nowadays increasingly more popular, particularly low-cost variants (Zheng et al., 2019; Mukherjee et al., 2019; Tanzer et al., 2019; Morawska et al., 2018). Their typical time resolution is between 1 s and 1 min, and because of their price and size, they can be used in networks to provide better spatial coverage (Martin et al., 2019; Li et al., 2019). Furthermore, they provide information about multiple mass fractions of particulate matter simultaneously, unlike the concentration of a single fraction in a gravimetric system or BAM. However, there are concerns about their suitability for measuring mass concentrations of ambient PM, since there is a significant measurement uncertainty arising from the principles of their operation.

Most commercially available OPS use Mie scattering theory (Mie, 1908) to determine the size and number of particles within the unit volume of air. Mie theory provides the solution of the Maxwell equations for the scattering of plane waves on spherical particles. The Mie solution is rather complex, but in order to illustrate the non-linearity of the theory, it will suffice to consider the case where particles are much smaller than the wavelength (of light, since a red laser is commonly used in practice). In that case the intensity of scattered radiation is given by

$$I = I_0 \frac{1 + \cos^2\theta}{2R^2} \left(\frac{2\pi}{\lambda}\right)^4 \left(\frac{d}{2}\right)^6 \left|\frac{m^2 - 1}{m^2 + 2}\right|^2, \quad (1)$$

where I_0 is the intensity of the incident radiation, θ is the scattering angle, R is the distance between the particle and the observing point, λ is the wavelength, d is the particle diameter and m is the refractive index of the particle. Thus, in order to calculate the diameter of the particle by measuring the intensity of the scattered radiation, one must assume a value for the refractive index of the particle. If the particle absorbs nothing from incoming radiation, its refractive index will be real; otherwise, it is written in the form

$$m = n + i\kappa, \quad (2)$$

where κ is called the extinction coefficient and is related to the absorption coefficient α :

$$\alpha = \frac{4\pi\kappa}{\lambda}. \quad (3)$$

Once the size distribution is calculated across K channels (bins), the total mass concentration of particles will be

$$c_m = \sum_{i=1}^K w_i \rho_i V_i N_i, \quad (4)$$

where V_i is the (average) volume, ρ_i is the density of the particles, N_i is the number of particles per unit volume and w_i is the weighting factor for channel i . Here we have another cause of OPS uncertainty: the density of particles must be assumed. Regarding the weighting factors, sensor manufacturers calculate values to correct for certain effects, such as the fact that OPS cannot detect particles which are too small.

Laboratory tests and calibrations of OPS are performed under controlled conditions with known particles, such as polystyrene latex spheres (Walser et al., 2017; Bezantakos et al., 2018), continuously changing monodisperse particles (Kuula et al., 2017; Kuula et al., 2020) or multi-modal particles (Cai et al., 2019). A burning chamber is used in some investigations as well (Wang et al., 2015). However, Eq. (1) is strongly non-linear in terms of refractive index, and in most practical cases corrections for different particles' optical properties are impossible to implement. Furthermore, densities appearing in Eq. (4) are not known a priori. That explains why it is difficult to calibrate OPS for realistic ambient PM concentration measurements: any laboratory calibration may or may not be applicable to the changing outdoor conditions (Tryner et al., 2020; Crilley et al., 2020).

For outdoor applications, there is an additional problem: hygroscopic growth of particles (Jayaratne et al., 2018; Granados-Muñoz et al., 2015; Di Antonio et al., 2018), which leads to overshoots of OPS if the ambient air humidity is (too) high. An obvious solution is to dry the air. However, any proper drying system would cost more than many models of OPS, and it is rarely seen in combination with low-cost sensors. Analytical corrections are often used: humidity sensors are used to measure the relative humidity of ambient air, and some analytical models, like Kohler's theory (Castarède and Thomson, 2018) or the Hänel equation (Hänel, 1976), are applied. Later in this paper we will make some observations on this issue.

Due to all the above-mentioned factors, it is always interesting to check how OPS perform in different realistic scenarios. Numerous papers deal with laboratory calibrations and outdoor evaluations of OPS (Karagulian et al., 2019; Borghi et al., 2018; Chatzidiakou et al., 2019; Magi et al., 2020; Sousan et al., 2016b; Malings et al., 2020; Kelly et al., 2017; Sayahi et al., 2019; Crilley et al., 2018; Zheng et al., 2018; Tasic et al., 2012; Cavaliere et al., 2018; Mukherjee et al., 2017; Sousan et al., 2016a; Zhang et al., 2018; Holstius et al., 2014; Badura et al., 2018). Reported results vary depending on the composition of particulate matter pollution, range of concentrations and meteorological factors. In Mukherjee et al. (2017) OPC-N2, PMS7003 and 11-R were compared against BAM-1020 during 12 weeks in the Cuyama Valley, California, USA. Grimm 11-R per-

formed well, while both OPC-N2 and PMS7003 (which is a miniaturized version of PMS5003) produced mediocre performance with heavy low bias. PurpleAir (PMS5003) was tested in Tryner et al. (2020) using laboratory and field tests. High bias of PMS5003 was observed. In Magi et al. (2020) PurpleAir (PMS5003) was analysed for 16 months in Charlotte, North Carolina, USA, against BAM-1022, and high bias of PMS5003 that increases with humidity was reported. High mean bias of PurpleAir (PMS5003) was reported in Kosmopoulos et al. (2020) as well.

The novelty of this research is a unique combination of instruments and conditions of extremely high urban pollution. The city of Sarajevo is situated in a valley and is affected by strong temperature inversions that appear typically 150–300 m above ground level with a very strong temperature gradient in the inversion layer, exceeding 30 K km^{-1} (Masic et al., 2019). The inversion episodes were present during most of January 2020. As a consequence, the average monthly concentration of $\text{PM}_{2.5}$ was very high: $167.3 \mu\text{g m}^{-3}$. In contrast to that, monthly average values for March and April 2020 were 21.6 and $19.6 \mu\text{g m}^{-3}$, respectively. This presented an excellent opportunity to test the performance of OPS in very different pollution levels. Simultaneously with OPS and reference gravimetric measurements, a scanning mobility particle sizer (SMPS) was employed to detect nanoparticles. It can detect particles with diameters from 10 nm up to $1 \mu\text{m}$. While an SMPS can count very small particles, 11-D can count larger particles, from 0.25 to $35 \mu\text{m}$ in diameter. When they work simultaneously, they can detect (almost) the full range of particles' diameters, with a span of more than 3 orders of magnitude. This will give detailed insights into the mass distribution of particles.

2 Methodology and experimental setup

The experimental facility was located at the Faculty of Mechanical Engineering in the central part of the Sarajevo valley (43.85424° N , 18.39607° E ; 540 m above sea level) and represents well the overall conditions in the city. The reference instrument for measurements of PM concentrations was a Dadolab Gemini air sampler (Fig. 1). It is a single device with two completely independent channels ($\text{PM}_{2.5}$ and PM_{10} in this campaign). The filter preparation and gravimetric analysis are performed in a separate laboratory of the Faculty of Science, Department of Chemistry. The air sampler, gravimetric laboratory and all filter procedures satisfied requirements of the standard EN 12341:2014. According to requirements of the standard, all filters were conditioned at relative humidity between 45 % and 50 % and temperature between 19 and 21°C .

The Grimm 11-D is a high-end optical particle sizer, with sophisticated construction and the ability to count individual particles from 250 nm to $35 \mu\text{m}$ in 31 equidistant (on logarithmic scale) channels. It uses a proprietary algorithm and

the manufacturer does not share information about the refractive index, density or weighting factors. It was factory calibrated and equipped with firmware version 12.50. Data were recorded in 1 min intervals (6 s is also possible). Since we use the common term OPS occasionally, it should be noted that 11-D belongs to a different category of devices (in comparison to low-cost sensors).

Alphasense OPC-N2 belongs to the category of low-cost sensors. The manufacturer transparently shared most specifications. It has a much simpler construction than 11-D: instead of a regulated pump, air flow is provided by a 25 mm fan. The device has 16 channels, from 380 nm to $17 \mu\text{m}$. Firmware version 18.2 was used. Refractive index was $n = 1.50 + i0$ and density was 1.65 g cm^{-3} . All other parameters, including weighting factors, were used as firmware default values.

The Plantower PMS5003 could be termed a very low-cost sensor, since its price is lower by an order of magnitude than that of the OPC-N2. Limited specifications do not reveal all operating parameters. From the specification sheet we can conclude that the device uses Mie scattering theory, with a detection limit of 300 nm, and has six channels. It uses a red semiconductor laser, a photodetector at a 90° scattering angle (Kuula et al., 2020) and a 32-bit processor (Cypress CY8C4245, 48 MHz). According to (Tanzer et al., 2019) PMS5003 is a nephelometer, not the particle counter. Air flow is provided by a 20 mm fan. The PMS5003 has two data outputs, one called SM (standard material, $\text{CF} = 1$) and another AE (atmospheric environment). The latter mode is used in our work, since the manufacturer recommends the AE mode for ambient air measurements, without further explanation. Figure 2 shows results from our laboratory test using the incense scents as the source of PM. Based on these results, the relationships between the SM and AE modes are

$$\text{SM}_{\text{PM}_{2.5}} = \begin{cases} \text{AE}_{\text{PM}_{2.5}} & \text{for } \text{AE}_{\text{PM}_{2.5}} \leq 30 \\ \text{non-linear} & \text{for } 30 < \text{AE}_{\text{PM}_{2.5}} \leq 50, \\ 1.5 \times \text{AE}_{\text{PM}_{2.5}} & \text{for } \text{AE}_{\text{PM}_{2.5}} > 50 \end{cases}$$

$$\text{SM}_{\text{PM}_{10}} = \begin{cases} \text{AE}_{\text{PM}_{10}} & \text{for } \text{AE}_{\text{PM}_{10}} \leq 43 \\ \text{non-linear} & \text{for } 43 < \text{AE}_{\text{PM}_{10}} \leq 77. \\ 1.5 \times \text{AE}_{\text{PM}_{10}} & \text{for } \text{AE}_{\text{PM}_{10}} > 77 \end{cases} \quad (5)$$

Based on PMS5003, we have designed a MAQS (Mobile Air Quality System) smart sensor. Essentially, it is a modular platform for PMS5003, with options for additional sensors (pressure, temperature, humidity, carbon dioxide, wind speed), GNSS receiver, flash memory, WiFi module and 3D-printed enclosure. Eight MAQS sensors were made and tested prior to the main campaign in order to evaluate consistency between units. Figure 3 shows the results of preliminary outdoor measurements for a batch of eight MAQS sensors. They showed very good consistency: the coefficient of determination, R^2 , between any two sensors from the batch was greater than 0.99, and average readings from all sensors are within $\pm 10\%$ from the average value of the batch of sen-

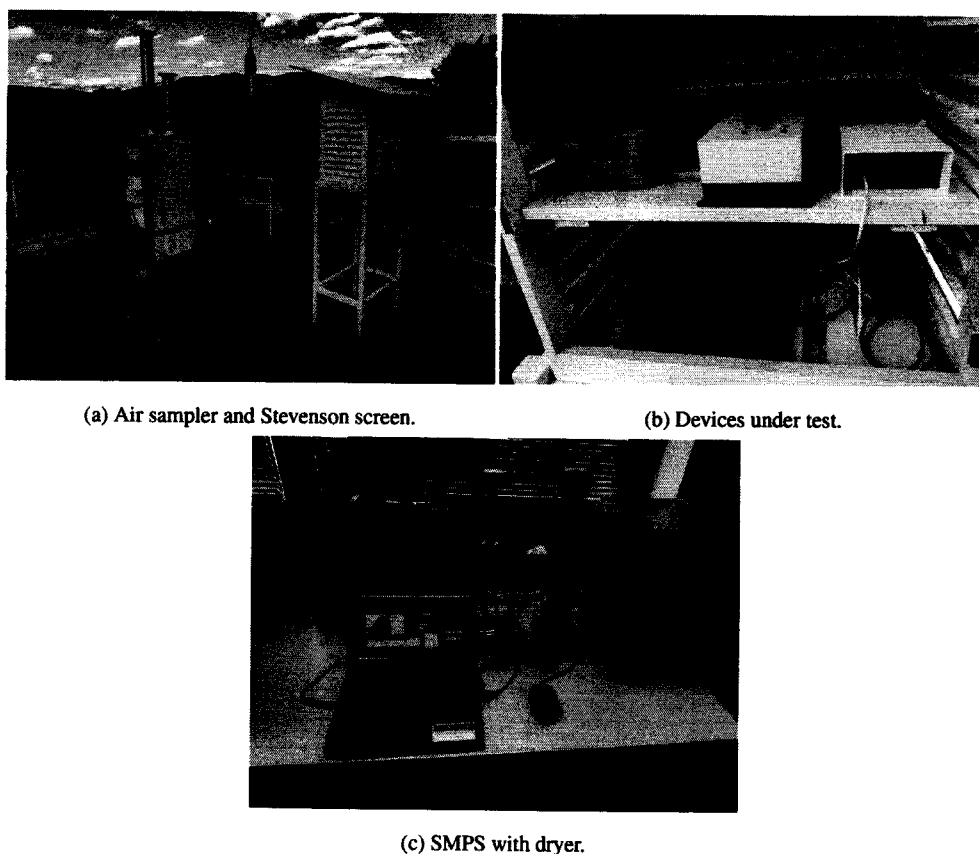


Figure 1. Experimental setup: (a) colocated air sampler and Stevenson screen; (b) devices under test inside of the Stevenson screen: 11-D with dryer, OPC-N2 with SPI adapter and (white-orange) enclosure, MAQS (white enclosure with grey front panel), and (c) indoor SMPS with dryer.

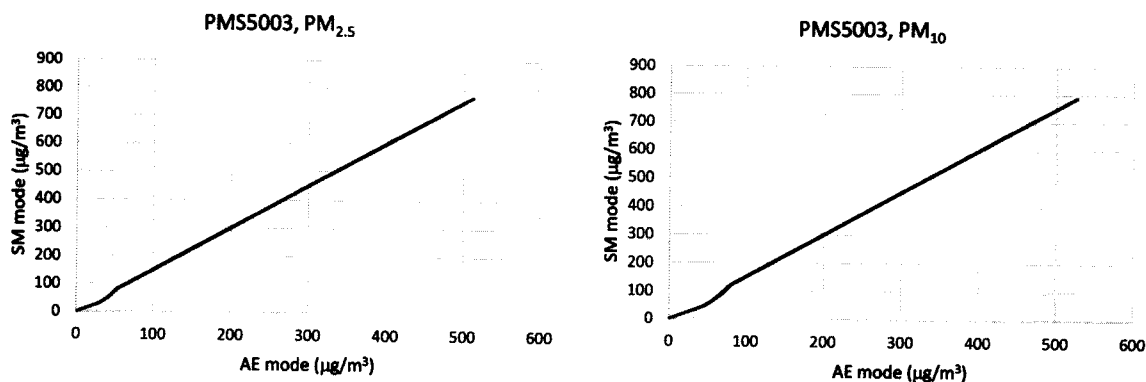


Figure 2. AE and SM modes of the PMS5003 sensor.

sors. Data were recorded every minute on a local SD card and remote cloud server simultaneously. The recording interval can be as short as 1 s, but there was no need for that.

The Grimm 11-D and Alphasense OPC-N2 could not be used outdoors without shelter, while MAQS has a special case which provides basic protection for outdoor use. Furthermore, a netbook PC was used to record data from the OPC-N2. Outdoor shelter had to be constructed to accom-

modate 11-D with power supply, OPC-N2 with PC and SPI adapter, and MAQS (for better protection). A Stevenson screen-like wooden structure was designed for that purpose. Another MAQS sensor was used at a remote location, for reasons that will be explained later.

For low-cost sensors (OPC-N2 and MAQS) there was no air dryer or heater, since they are typically used in such conditions. We have designed and constructed a diffusion dryer

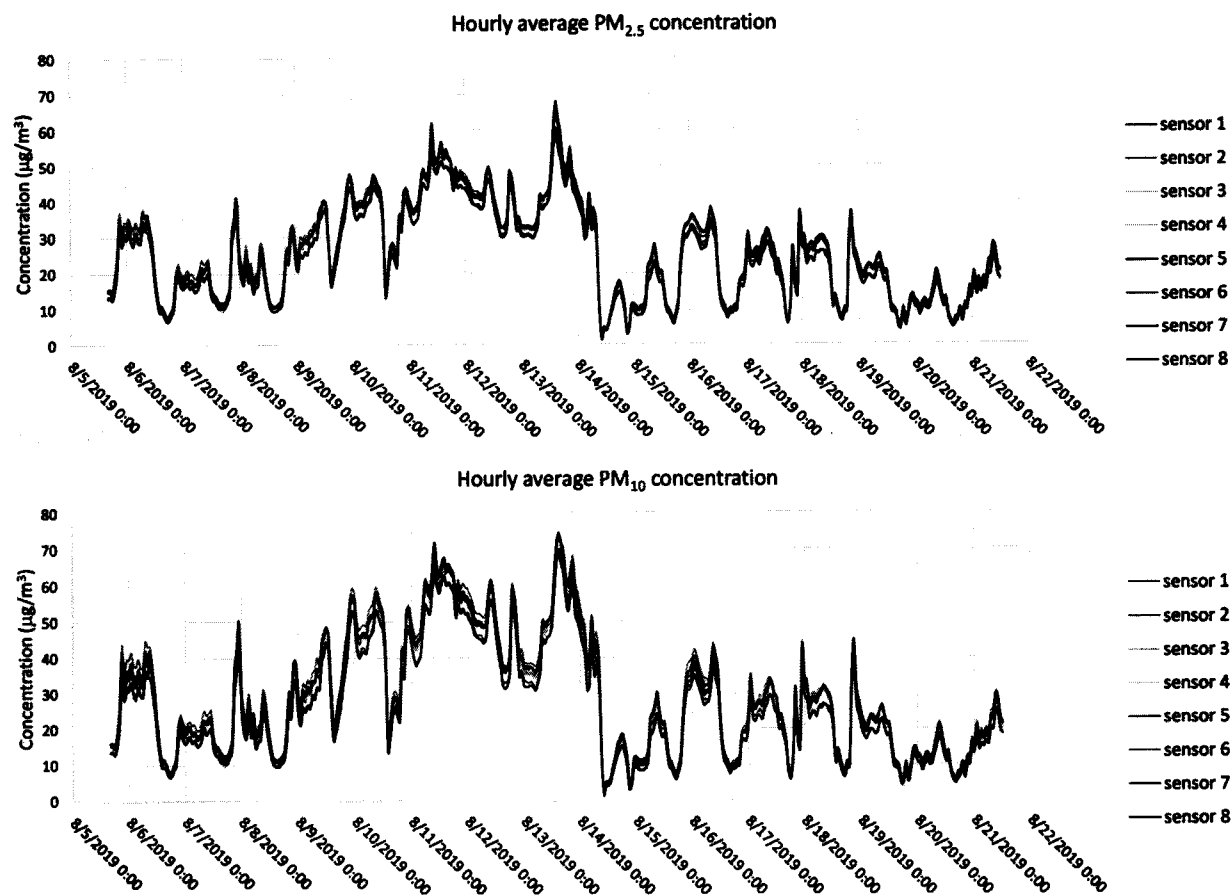


Figure 3. Preliminary test of eight MAQS sensors, outdoor measurements.

for application on 11-D, which consists of a porous stainless steel tube surrounded with 1 kg of silica gel. The dryer is compact, 25 cm in length with an 8 cm external diameter, and does not reduce the mobility of the instrument. It was installed only during the period of mild pollution.

Meteorological parameters were measured using the Vantage Pro2 (Davis Instruments, USA) weather station with recording intervals of 15 min.

An SMPS is a complex system which consists of a condensation particle counter (CPC), a differential mobility analyser (DMA) and a charge conditioner (often inadequately called a “neutralizer”). Depending on the characteristics of the DMA, the SMPS can be configured for a certain span of particle diameters. We have used a Grimm 5.416 high-end SMPS with a long DMA which is able to separate particles from 10 to 1000 nm into 129 channels, equidistant on a logarithmic scale. Despite the fact that particles with diameters below 10 nm play an important role in nucleation and growth studies (Tiszenkel et al., 2019), their contribution to the mass budget is negligible. Another (larger) in-house developed diffusion dryer was installed at the inlet of the SMPS. A soft X-ray device was used as the charge conditioner. Scanning mode (alternating upscan and downscan) was used for all

measurements. One scan takes about 4 min (8 min for both upscan and downscan). When working in parallel, the SMPS and 11-D form a powerful wide-range spectrometer, which covers a range of particle diameters from 10 nm to 35 µm in 160 channels. Additionally, there is an overlapping area between 250 and 1000 nm where we can see how well these two instruments match. The complex SMPS system was kept indoors (an unavoidable necessity, since both X-ray charger and DMA use very high operating voltages). The air was sampled from outside using a conductive tube of the shortest possible length to avoid particle losses. It was running continuously, except for the periods of maintenance.

A rigorous data validation procedure was used. All instruments were inspected periodically and data logs were analysed thoroughly. When calculating daily average values, complete and consistent data series were required.

3 Results and discussion

During this campaign 296 filters were used in the reference air sampler. After the removal of several blank filters used for periodic verification and those with incomplete sampling (the pneumatic system of the air sampler failed to load new

filters automatically a couple of times), 288 filters remained: 143 PM_{2.5} and 145 PM₁₀ samples. Figure 2 shows PM_{2.5} and PM₁₀ daily average concentrations, together with hourly and daily values of ambient air temperature and relative humidity.

Some modifications of the shelter for 11-D and OPC-N2 were necessary, making those instruments unavailable periodically during December and January. Additionally, more frequent maintenance, such as cleaning of 11-D, was needed when working in extreme conditions. The same goes for the SMPS, which was maintained according to the recommendations of the manufacturer. Taking into account difficult operating conditions, the amount of data collected is satisfactory during the period of strong pollution and excellent during the period of mild pollution. The lower limit of detection (LLoD) of PM_{2.5} concentration for evaluated optical aerosol devices is estimated based on their actual field performance. Standard deviation (σ) was calculated for periods with near-zero ambient PM concentration, and an average value of 3σ is the estimated LLoD. For PMS5003 our final estimation is $5 \mu\text{g m}^{-3}$. The same value is an estimation of Magi et al. (2020), calculated by averaging segmented regressions, and Bulot et al. (2019), by combining results from several previous studies. This method applied to OPC-N2 yields an LLoD of 2 and $1 \mu\text{g m}^{-3}$ for 11-D. For the reference gravimetric system LLoD was calculated using the blank filters, which were treated in exactly the same way as real samples (except the sampling of particulate matter), and the calculated value of LLoD is $0.7 \mu\text{g m}^{-3}$. All measurements below LLoD were discarded during the quality assurance phase.

3.1 Strong urban pollution

During the period of strong urban pollution (2 December 2019–12 March 2020), the average value of PM_{2.5} concentration was $82.9 \mu\text{g m}^{-3}$, with minimum daily average value $1.3 \mu\text{g m}^{-3}$ and maximum value $504.9 \mu\text{g m}^{-3}$ (Fig. 4). In the same period, the average PM₁₀ concentration was $95.5 \mu\text{g m}^{-3}$, with minimum value $3.6 \mu\text{g m}^{-3}$ and maximum value $549.0 \mu\text{g m}^{-3}$. The ratio of average values of concentrations PM_{2.5}/PM₁₀ was 0.87. Very good correlations were observed for all three OPS against the reference instrument (Fig. 5). Such a range of ambient PM concentrations was favourable for achievement of high R^2 values, but non-linear effects of low-cost sensors were observed too.

The Grimm 11-D produced results with R^2 values of 0.988 and 0.985 for PM_{2.5} and PM₁₀ concentrations, respectively. Absolute values were larger than the reference, on average 17.6 % for PM_{2.5} and 25.5 % for PM₁₀. The average ratio PM_{2.5}/PM₁₀ measured by 11-D was 0.93. Mean absolute error (MAE) was $13.4 \mu\text{g m}^{-3}$ for PM_{2.5} and $10.8 \mu\text{g m}^{-3}$ for PM₁₀. Alphasense OPC-N2 undershoots with respect to the reference values, on average 31.0 % for PM_{2.5} and 36.8 % for PM₁₀, but R^2 coefficients are relatively high: 0.903 and 0.920 for PM_{2.5} and PM₁₀, respectively. The OPC-N2 measured the ratio PM_{2.5}/PM₁₀ to be 0.97. MAE for this sen-

sor was $29.4 \mu\text{g m}^{-3}$ for PM_{2.5} and $34.8 \mu\text{g m}^{-3}$ for PM₁₀. The MAQS sensor produced surprisingly good R^2 values of 0.975 for PM_{2.5} and 0.950 for PM₁₀. In terms of absolute values, it overshoots by 31.9 % for PM_{2.5} and 49.3 % for PM₁₀ (on average). The calculated ratio PM_{2.5}/PM₁₀ was 0.76. MAE was $35.9 \mu\text{g m}^{-3}$ for PM_{2.5} and $55.2 \mu\text{g m}^{-3}$ for PM₁₀. It seems that the Plantower PMS5003 cannot accurately determine the PM₁₀ fraction. One possible explanation is provided by a laboratory test of PMS5003, where it was found that its size bin [2.5–10 μm] is noisy and inaccurate (Kuula et al., 2020). Further investigation of this behaviour would be useful.

None of the tested OPS were equipped with an air dryer, and this certainly contributes to overprediction. However, Alphasense OPC-N2 with default firmware settings underpredicts values, despite the particle hygroscopic growth effect.

3.2 Mild urban pollution

The correlation coefficients changed dramatically in the period of mild pollution (13 March 2020–4 May 2020), as Fig. 6 shows. The much narrower range of particulate matter concentrations plays an important role, and even the reference method is less accurate, since the mass difference of loaded and blank filters becomes very small (smaller than 1 mg for the 24 h sampling period if PM concentration is below $18 \mu\text{g m}^{-3}$). The average concentration of PM_{2.5} was $19.7 \mu\text{g m}^{-3}$ with a minimum daily average value of $7.1 \mu\text{g m}^{-3}$ and a maximum value of $39.3 \mu\text{g m}^{-3}$. During this period, the average value of the PM₁₀ concentration was $24.2 \mu\text{g m}^{-3}$, with minimum and maximum values of 7.6 and $48.8 \mu\text{g m}^{-3}$, respectively. The ratio PM_{2.5}/PM₁₀ was 0.81 on average.

This time the Grimm 11-D was equipped with a dryer, whose effects will be discussed in the next subsection. The device produced relatively high R^2 values of 0.868 for PM_{2.5} and 0.917 for PM₁₀. The absolute readings underestimated concentrations of PM_{2.5} by 16.3 % on average, while PM₁₀ were underestimated by 10.9 % on average. The PM_{2.5}/PM₁₀ ratio was 0.87. This test clearly shows that 11-D is a completely different class of instrument (in comparison to low-cost sensors). When equipped with a dryer, 11-D shows a level of performance comparable to BAM, at least those reported by Hafkenscheid and Vonk (2014). MAE was $3.0 \mu\text{g m}^{-3}$ for PM_{2.5} and $4.1 \mu\text{g m}^{-3}$ for PM₁₀.

Alphasense OPC-N2 did not perform well during the period of mild pollution. Coefficients of determination, R^2 , were only 0.284 for PM_{2.5} and 0.525 for PM₁₀. Absolute readings are worrying: the OPC-N2 underpredicted PM_{2.5} by 67.6 % and PM₁₀ by 71.6 % on average. The ratio PM_{2.5}/PM₁₀ was 0.73. MAE was $13.8 \mu\text{g m}^{-3}$ for PM_{2.5} and $15.8 \mu\text{g m}^{-3}$ for PM₁₀.

The MAQS sensor demonstrated mediocre performance, with R^2 values of 0.730 for PM_{2.5} and 0.718 for PM₁₀. On average, this sensor overpredicted PM_{2.5} by 30.5 % and

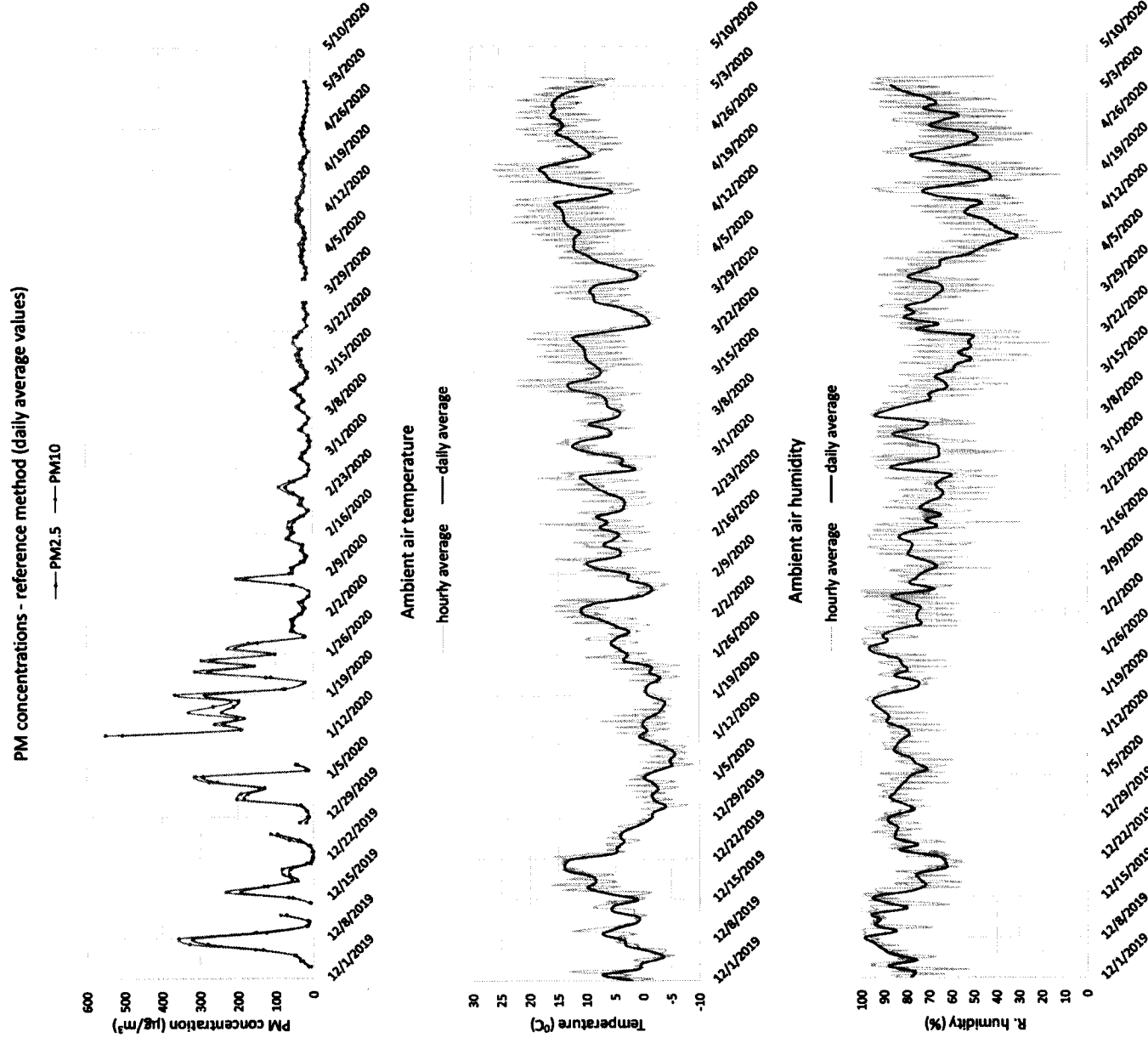


Figure 4. Reference PM concentrations with ambient air temperature and humidity.

PM₁₀ by 32.6 %. The PM_{2.5} / PM₁₀ ratio was 0.83, very close to the reference value (in contrast to the performance of the sensor in the period of strong pollution). MAE was $7.1 \mu\text{g m}^{-3}$ for PM_{2.5} and $8.2 \mu\text{g m}^{-3}$ for PM₁₀.

It would be interesting to test low-cost sensors with a proper dryer as well, but that combination is rarely seen in practice.

3.3 Humidity influence

One of the important factors in ambient measurements of PM concentrations is humidity, since the particles reflect more light (i.e. appear larger) during measurements due to hygroscopic growth. This can be described using the Hanel equation:

$$f_{\zeta}(\text{RH}) = \left(\frac{1 - \text{RH}}{1 - \text{RH}_{\text{ref}}} \right)^{-\gamma}, \quad (6)$$

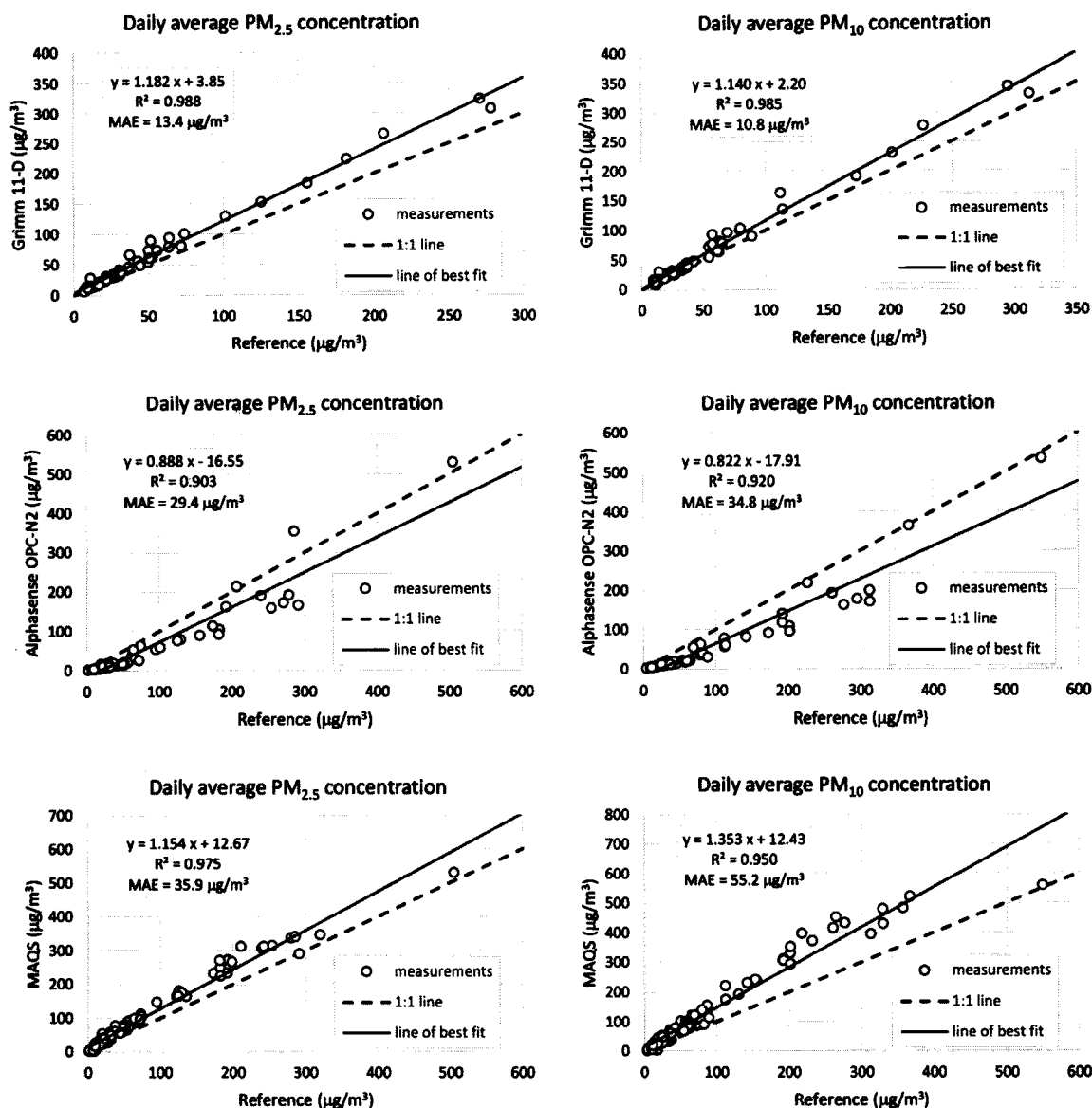


Figure 5. OPS performance during the period of strong pollution (2 December 2019–12 March 2020).

where f_{ζ} is the enhancement factor for particle property ζ . Here RH represents the relative humidity and RH_{ref} is a reference relative humidity:

$$f_{\zeta}(\text{RH}) = \frac{\zeta(\text{RH})}{\zeta(\text{RH}_{\text{ref}})} \quad (7)$$

It is important to note that the coefficient γ , which is an indicator of the hygroscopicity of particles, depends on the type of particles (and changes whenever the composition of ambient particles is changed).

If we compare results produced by 11-D relative to the reference, during period 1 (without a dryer) and period 2 (with a dryer), we can see that readings of 11-D were reduced by more than 30%. However, we cannot conclude whether it was the effect of the dryer or the consequence of signifi-

cantly different ambient conditions. Unfortunately, we have only one 11-D, so we could not measure simultaneously with and without a dryer (that is the reason why we used the instrument with the dryer only in one of the two periods). If we take into account two intervals with similar ambient conditions, with and without a dryer we get the following values: from 27 February 2020 to 12 March 2020 the average ambient concentration of PM_{2.5} was $21.1 \mu\text{g m}^{-3}$, while 11-D (without a dryer) measured 21.5% more. In the second interval, from 13 March 2020 to 1 April 2020, the ambient concentration was similar, $21.0 \mu\text{g m}^{-3}$, while 11-D (with a dryer) measured a 1.4% smaller value. This comparison indicates that the effect of the dryer could be around 23%. A similar analysis for PM₁₀ concentrations gives an estimate of about 20% for the dryer effect.

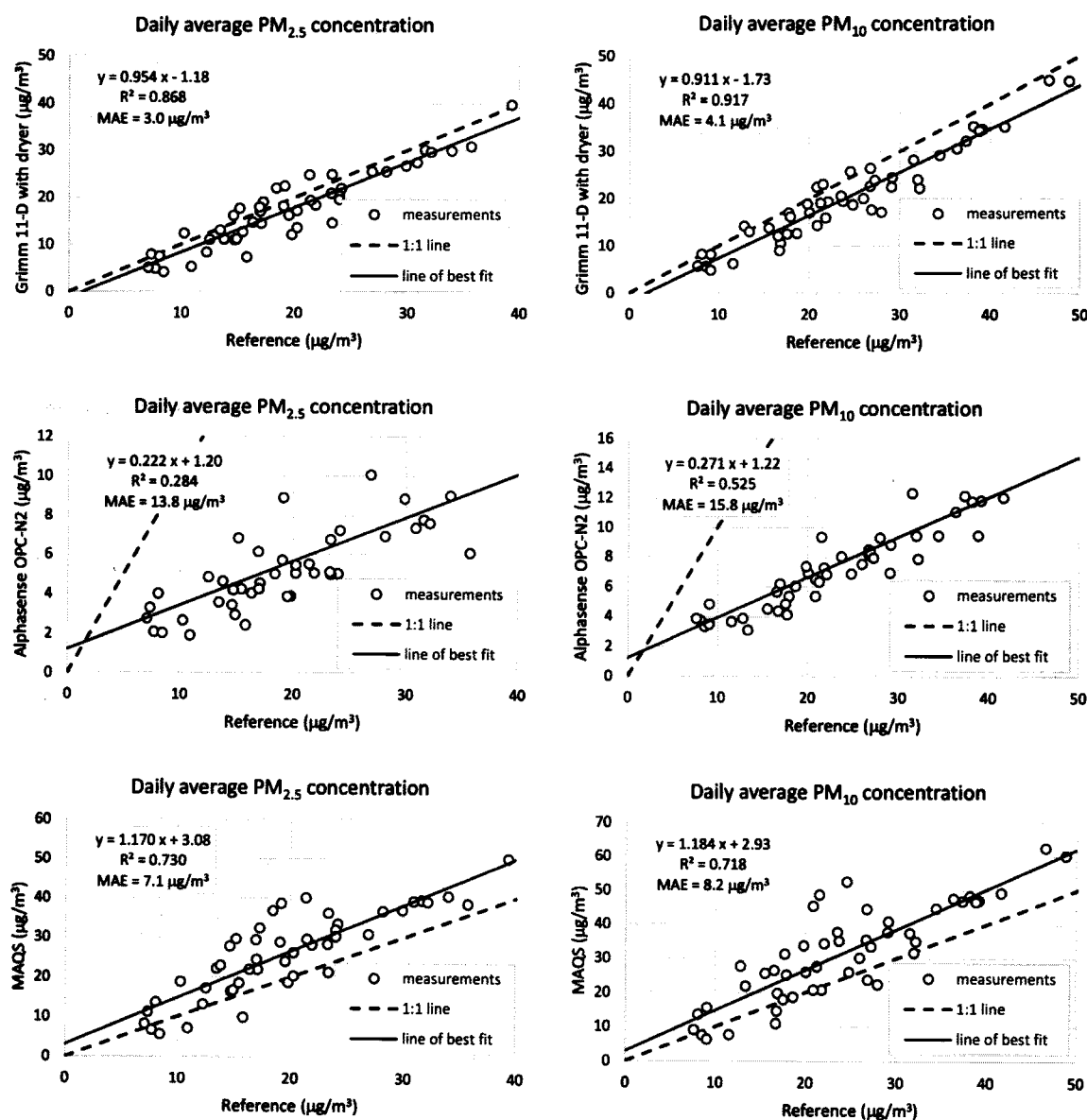


Figure 6. OPS performance during the period of mild pollution (13 March 2020–4 May 2020).

The Grimm 11-D has a very useful feature: an internal temperature and humidity sensor. Figure 7 shows the self-heating and diffusion dryer effect on 11-D by comparing internal and external measurements of temperature and humidity. The average ambient air temperature from 27 February 2020 to 1 April 2020 was 7.02 °C, while the average 11-D internal temperature was 14.27 °C, which shows a significant difference of 7.25 °C. This self-heating effect reduces internal humidity significantly, and we can see that it rarely goes beyond 50 %. Once the dryer is installed, internal relative humidity is further reduced: the average value of internal humidity without a dryer (27 February 2020–12 March 2020) was 36.2 %, and with a dryer (13 March 2020–1 April 2020) it was 21.8 % (the ambient air humidity also dropped

in the later period, but nevertheless the effect of the dryer is evident).

After roughly a month, the dryer's performance degraded and the silica gel needed a regeneration (but it was not performed since we did not want to interrupt measurements when the end of the campaign was near).

Figure 8 shows the long-term (13.5-month) comparison of MAQS and BAM-1020 with a time resolution of 1 h, together with measured values of ambient air humidity. By averaging all these data we can estimate the influence of humidity on the MAQS sensor: if we sort the measurements by humidity, a subset of points where humidity is below 50 % has an average bias of 14.3 %, for humidity range 50 %–70 %, bias is 16.5 %, for humidity range 70 %–85 %, bias is 31.6 % and for humidity range 85 %–100 %, bias is 37.3 %. If we sub-

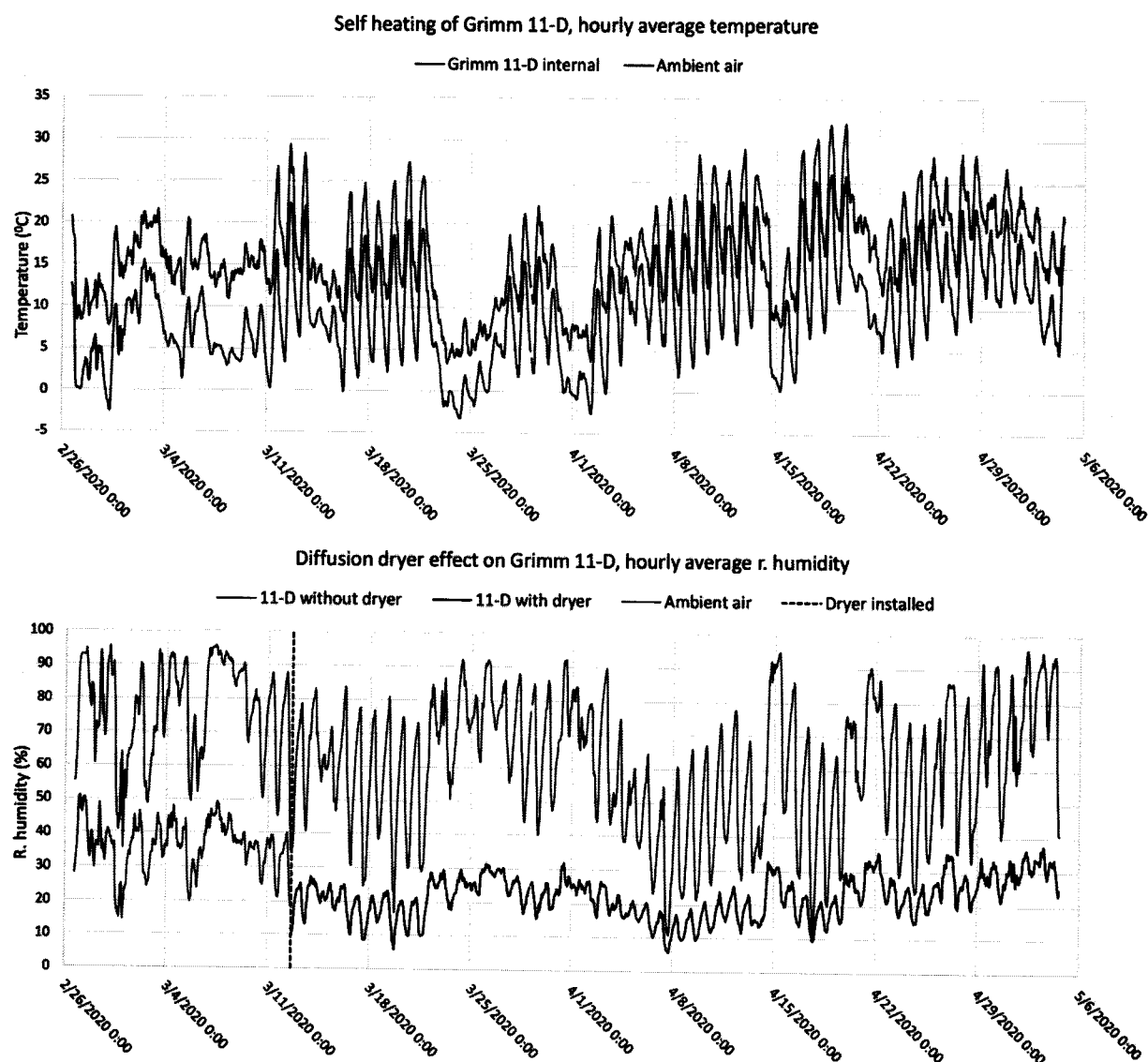


Figure 7. Self-heating and diffusion dryer effect of the Grimm 11-D. The dryer was installed on 12 March 2020 15:30 LT (UTC+1).

tract the bias of the least humidity subset from the bias of the highest humidity subset, we can estimate that humidity influence adds up to 23 % on $PM_{2.5}$ readings from the MAQS sensor, which is a similar result to the analysis of humidity influence on our 11-D with dryer installed. While this influence cannot be neglected, it is still relatively modest. A possible reason is the chemical composition of PM without too many hygroscopic components, but that requires a different type of analysis. A relatively modest humidity influence on PMS5003 was also reported in Jayaratne et al. (2018), and a surprisingly low influence is reported by Kosmopoulos et al. (2020).

3.4 SMPS data and wide-range spectrometer

The wide-range spectrometer (SMPS+11D) produced very valuable results. Figure 9 shows the continuous concentra-

tion and mass distributions. It is created from hourly average measurements from the SMPS and 11-D. A relative density of 1.65 was applied in SMPS software (based on LabVIEW) for the mass calculation. No other corrections were performed and all settings were factory defaults. Selected histograms (hourly average values) are shown in Fig. 10. What we can see from Figs. 9 and 10 is that in the period of strong pollution the dominant mass contribution comes from particles with diameters around 300 nm. In terms of concentrations, particles around 100 nm appear in the greatest numbers, with occasional secondary peaks coming from even smaller particles.

In the period of mild pollution, however, we can see that particles larger than $2.5 \mu\text{m}$ often appear on histograms (usually about $3 \mu\text{m}$ in diameter). Number concentrations still have peaks of about 100 nm, but sometimes the distribution

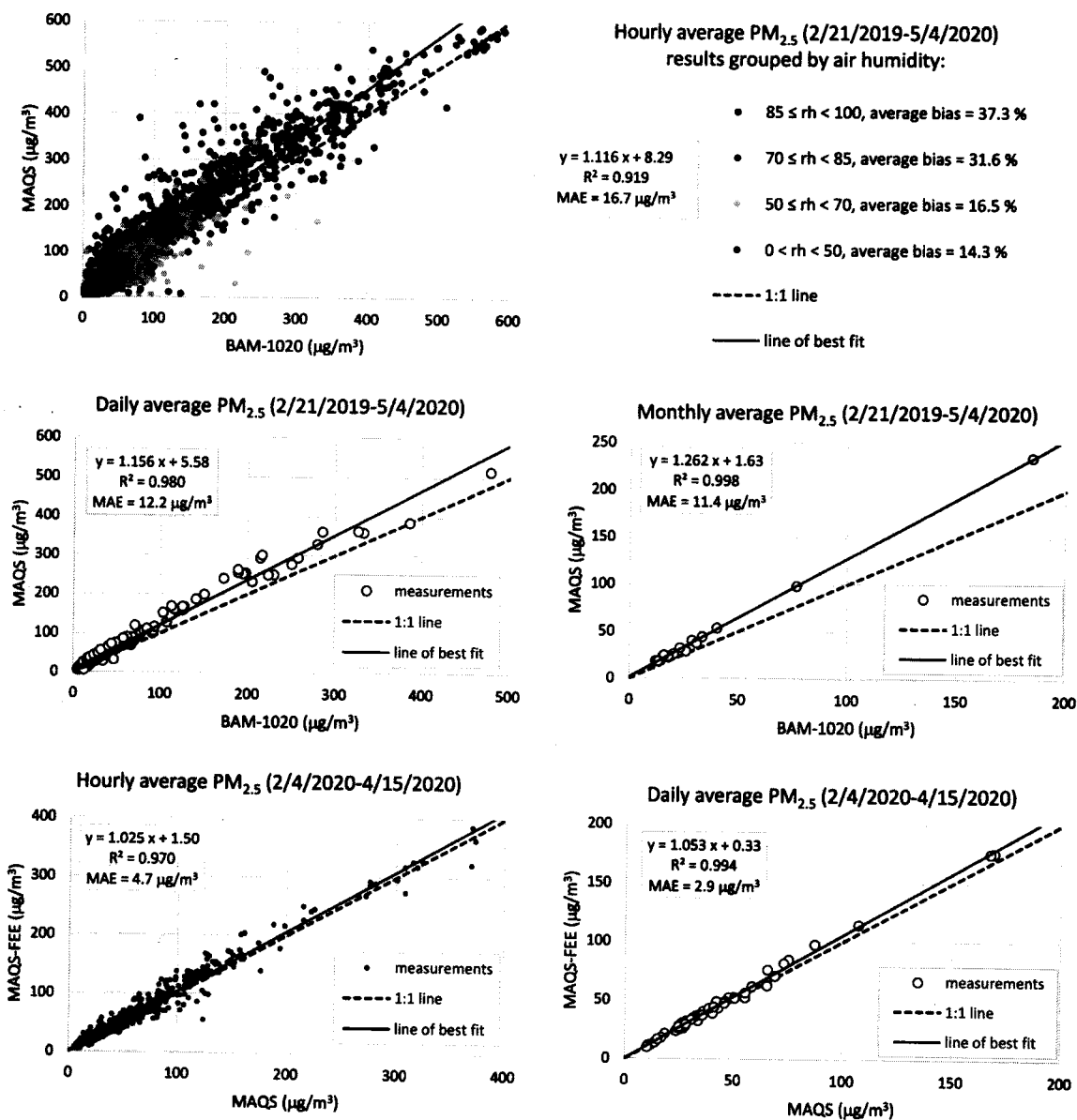


Figure 8. Long-term comparisons of the MAQS sensor with BAM operated by the US EPA at the nearby location: hourly, daily, and monthly average values and comparison of hourly and daily average values of two MAQS sensors: the first one (MAQS) at our main facility and the second one (MAQS-FEE) at the Faculty of Electrical Engineering in the immediate vicinity of BAM-1020.

is different in favour of even smaller particles, as Fig. 10 shows. Again, the largest mass contribution comes from particles around 300 nm.

In the overlapping area, the SMPS and 11-D matched very well, almost perfectly for concentrations. Their match was not as good for mass calculations, but that is understandable, taking into account all the factors explained in Sect. 1. Overall, the combination of the SMPS and 11-D worked very well and gave the full spectrum of particles, both for number concentrations and mass distribution.

The obtained mass distribution of particles, especially during the period of strong pollution, raises the question of the suitability of OPS for measuring mass concentrations and

resolving different fractions, since they cannot detect small particles that significantly contribute to the total mass. For example, the Alphasense OPC-N2 has a detection limit of 380 nm and cannot detect the particles around 300 nm which form the dominant contribution to the mass budget. The Grimm 11-D, with a detection limit of 250 nm, has a far better potential to resolve mass fractions.

3.5 OPS histograms and Aralkum Desert dust

All tested OPS have data bins, with different numbers of channels, as described in Sect. 2. Figure 11 shows histograms that compare data bins from 11-D, OPC-N2 and MAQS on

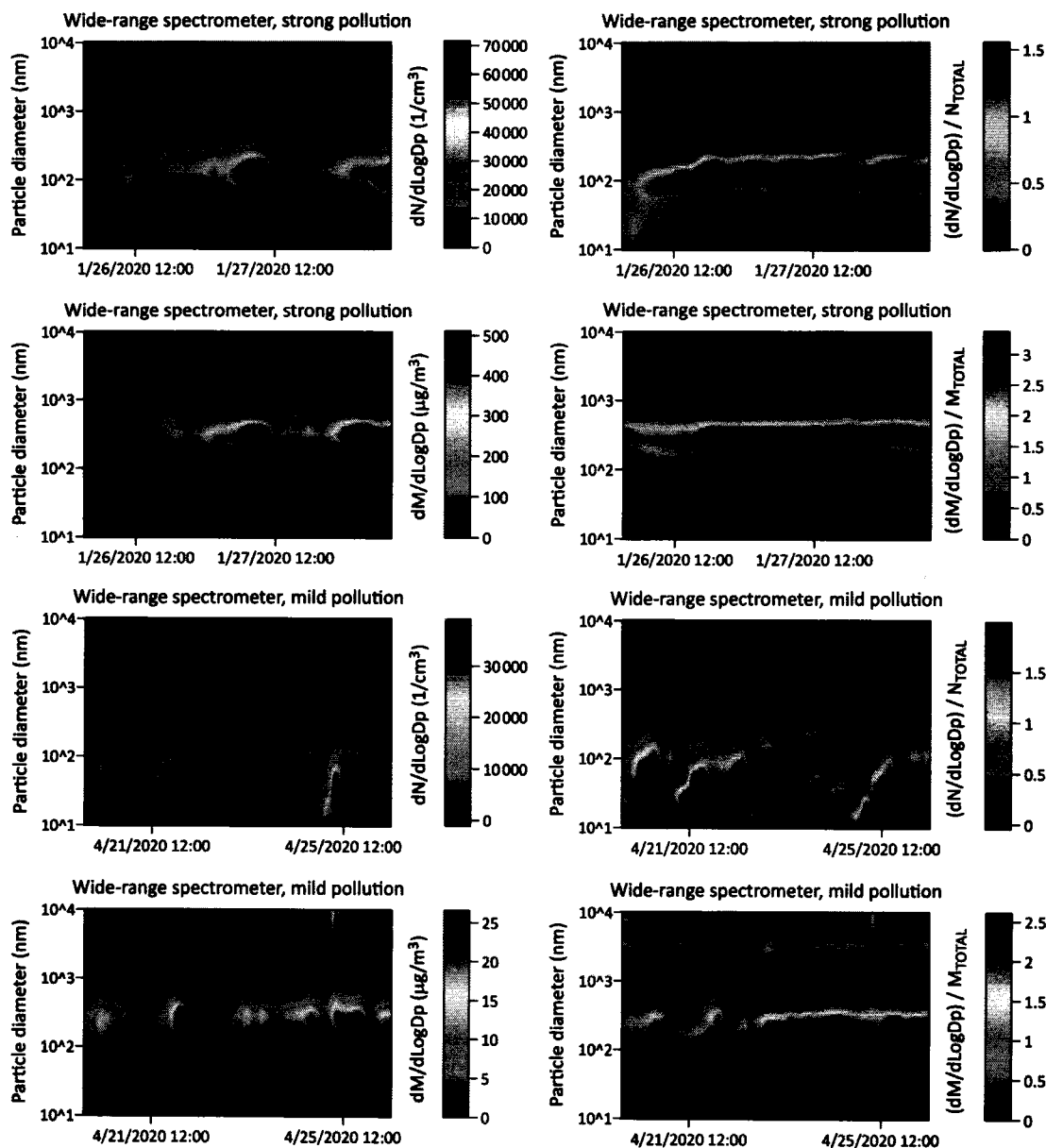


Figure 9. Wide-range spectrometer (SMPS+11D) and hourly average values. Relative density 1.65 was applied to the SMPS to calculate mass of particles.

18 January 2020 (strong pollution) and 16 April 2020 (mild pollution). It should be noted that we compare here data bins from devices with different specifications and categories. As expected, 11-D has the ability to count particles below 300 nm, which appear in the greatest numbers. Counting efficiency of OPC-N2 is investigated in laboratory conditions using PSL particles in Sousan et al. (2016a), and the results were good for particles larger than 0.8 μm , while for particles with a diameter of 0.5 μm OPC-N2 the device showed a lower detection efficiency (the detection limit of OPC-N2 is 0.38 μm). In our realistic scenario, the dominant contribution to the mass comes from particles much smaller than 0.8 μm (Figs. 9 and 10), which is not favourable to OPC-N2.

In contrast to OPC-N2, PMS5003 has problems with coarse particles, as indicated in laboratory tests (Kuula et al., 2020). If the fraction of coarse particles is small and steady, PMS5003 performs much better. Ambient conditions in Bosnia-Herzegovina are such most of the time, since the primary source of PM is combustion of coal and biomass. That could explain why PMS5003 performs better than OPC-N2 most of the time. However, different conditions were observed on 27 March 2020, when the dust from the Aralkum Desert covered part of Europe, including our test location. During this episode, OPC-N2 performed much better than PMS5003, which was not able to determine a large fraction of coarse particles correctly (Fig. 11). A similar observation

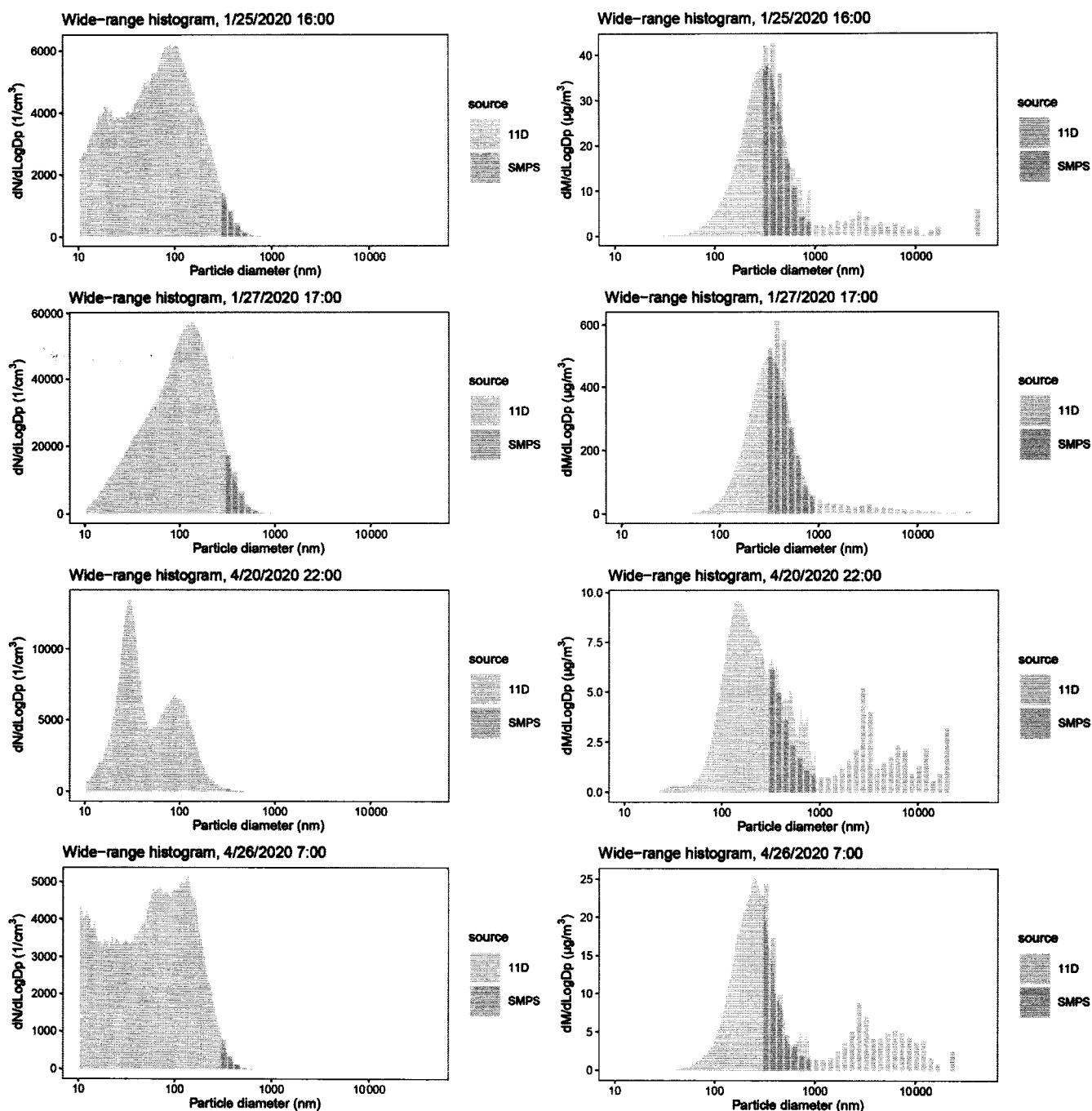


Figure 10. Wide-range histograms and hourly average values. Relative density 1.65 was applied to the SMPS to calculate mass of particles.

about PMS5003 was reported by Kosmopoulos et al. (2020), when Sahara dust covered Greece.

3.6 Long-term performance

Another question about OPS, especially low-cost types, is the drift of performance over time. The PMS5003 sensor uses a semiconductor laser (diode laser) which has a limited lifetime. We have some long-term comparisons of the

MAQS sensor with MetOne BAM-1020 operated at a nearby location by the US EPA. Strictly speaking, their station is not collocated with our equipment, but for a distance of only 300 m it is reasonable to assume that the air composition is very similar at these two points, since they are located in the same neighbourhood. In order to verify that assumption, we have installed another MAQS sensor at the location of the Faculty of Electrical Engineering, University of Sarajevo, which is in the immediate vicinity of the US

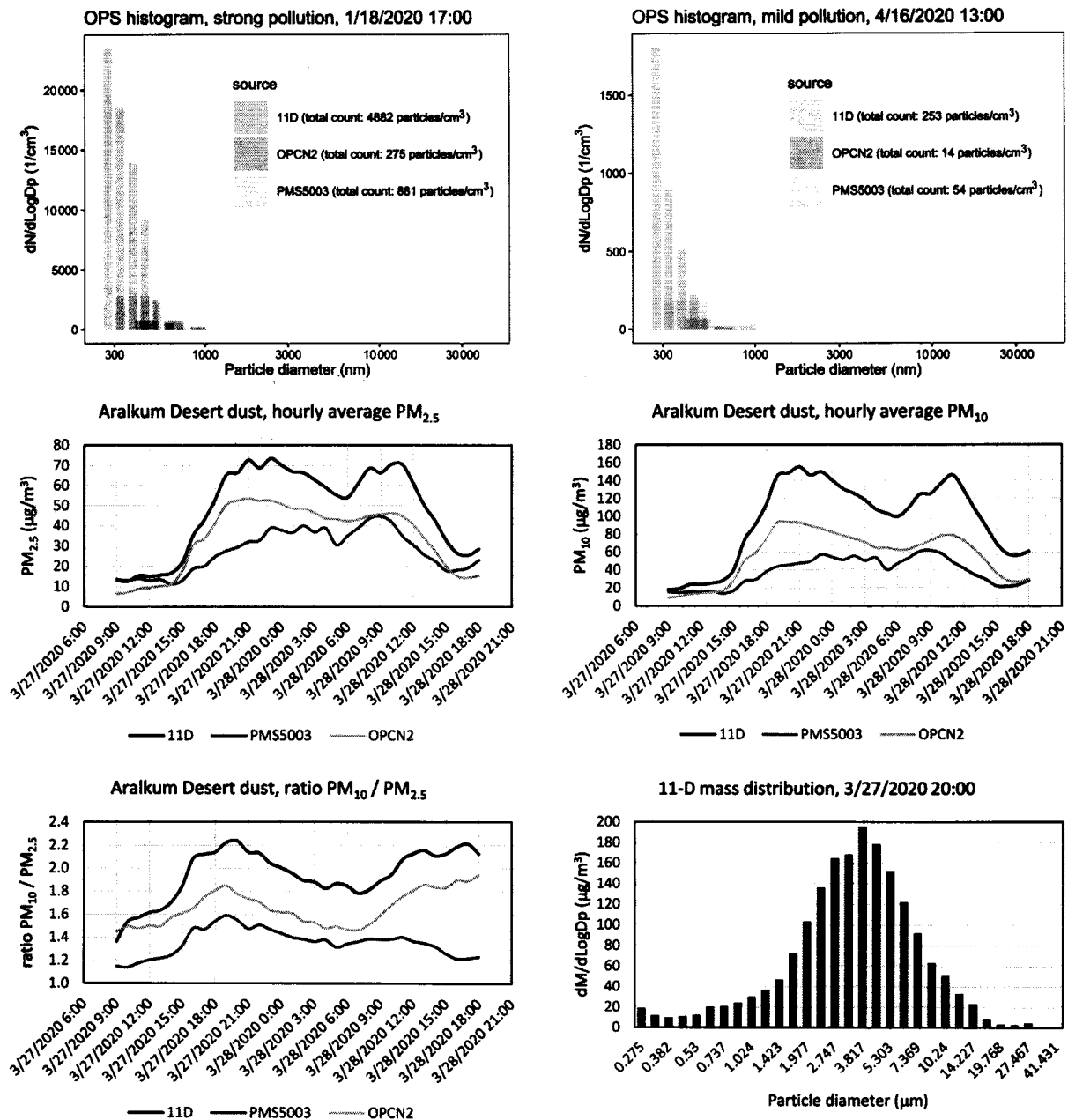


Figure 11. OPS histograms and Aralkum Desert dust episode, hourly average values.

EPA site and at the same distance from us (about 300 m). Figure 8 shows long-term comparisons of the MAQS sensor and BAM-1020 and additional verification of correlation between readings of the two MAQS sensors, which is very high ($R^2 = 0.970$, $MAE = 4.7 \mu\text{g m}^{-3}$ for hourly average values and $R^2 = 0.994$, $MAE = 2.9 \mu\text{g m}^{-3}$ for daily average values), confirming our assumption that these two locations share the same air in terms of PM concentrations and properties.

Based on 13.5 months of continuous comparison of MAQS and BAM-1020, hourly average values give R^2 coefficient 0.919 and $MAE = 16.7 \mu\text{g m}^{-3}$. Daily average val-

ues produce R^2 coefficient 0.980 and $MAE = 12.2 \mu\text{g m}^{-3}$, while the monthly average values give $R^2 = 0.998$ and $MAE = 11.4 \mu\text{g m}^{-3}$ (Fig. 8).

This leads us to the conclusion that time averaging reduces by a lot the influence of variation of PM composition and meteorological variations. If we use a longer time-average period, we lose one of the major advantages of low-cost sensors (time resolution), but it is a more natural approach to correcting readings compared to using artificial algorithms like neural networks (Badura et al., 2019) or machine learning (Si et al., 2020). An excellent viewpoint of this issue is given by Hagler et al. (2018). The calibration of a larger num-

ber of low-cost sensors can be simplified if they show similar relative performance (to each other) in the laboratory and field (Sousan et al., 2018). Floating corrections, even physically justifiable interventions, such as the instantaneous correction for humidity growth of particles, insert a lot of noise, and the benefit is questionable. Depending on ambient conditions, self heating of the sensor and some other factors, relative humidity may not be accurately determined. Even if we have a very accurate humidity measurement, the hygroscopic growth coefficient will change whenever the composition of PM changes, inevitably injecting noise into the results.

We can also see strong non-linear effects at very high concentrations, above $500 \mu\text{g m}^{-3}$. In that case a quadratic regression fit will be more suitable.

During this period of 13.5 months of continuous outdoor operation, the MAQS sensor worked flawlessly without performance drifts. Designed enclosure sufficiently protected the sensor outdoors while not obstructing air sampling.

4 Conclusions

A comprehensive experimental study was carried out with the aim of evaluating the performance of three very different OPS: high-end Grimm 11-D, low-cost Alphasense OPC-N2 and in-house developed MAQS sensor, which is based on another low-cost sensor, the Plantower PMS5003 sensor. The study was performed in realistic conditions of strong and mild urban pollution. The reference instrument was a dual-channel air sampler with gravimetric analysis in a separate laboratory. In total 288 filters were collected from 2 December 2019 to 4 May 2020.

During the period of strong urban pollution all three instruments produced very high R^2 values. However, during the period of mild urban pollution, these correlation factors dropped significantly, especially for the Alphasense OPC-N2 sensor measuring the $\text{PM}_{2.5}$ parameter. The OPC-N2 underestimated the mass concentrations badly, especially during the period of mild pollution. The MAQS sensor overshoots $\text{PM}_{2.5}$ concentrations by approximately 30% on average, which is partially caused by hygroscopic growth.

The wide-range spectrometer, which consists of the SMPS and 11-D, produced valuable information about the distribution of particles, both in number and mass concentrations. Particles with diameters around 100 nm (and sometimes below) represent the dominant fraction in pure numbers, while particles with diameters of around 300 nm give the highest contribution to mass. In the period of mild pollution, particles larger than $2.5 \mu\text{m}$ gave a larger contribution than in the period of strong pollution.

The Grimm 11-D performed well in all conditions, and when equipped with a dryer, it performed at a comparable level to the beta attenuation monitor. For the calibration of low-cost sensors, especially those based on PMS5003, we propose a linear or quadratic correction (in the case of high

pollution levels) with steady coefficients, since the instantaneous corrections insert noise into results.

Future measurements should further investigate characteristics of OPS in different ambient conditions, influence of humidity and effect of micro-dryers specifically designed for low-cost sensors and mass distributions by means of wide-range spectrometers.

Data availability. The underlying datasets for this publication are available at <https://doi.org/10.5281/zenodo.3897379> (Masic et al., 2020). Furthermore, data from the BAM measurements by the US EPA are available at <https://www.airnow.gov/?city=Sarajevo&country=BIH> (U.S. EPA, 2020).

Author contributions. AM participated in all phases of this research and wrote the manuscript with contributions from all the co-authors. DB and BP performed field work together with AM. AB designed, manufactured and analysed the performance of two diffusion dryers and evaluated the influence of humidity on the readings of 11-D. SZ and JH performed gravimetric measurements, including preconditioning and treatment of the filters, ensuring strict fulfilment of the standard EN 12341:2014.

Competing interests. The authors declare that they have no conflict of interest.

Acknowledgements. We would like to thank the Embassy of Sweden in Bosnia-Herzegovina for supporting this research and the United States Environmental Protection Agency for sharing data publicly.

Review statement. This paper was edited by Pierre Herckes and reviewed by three anonymous referees.

References

- Badura, M., Batog, P., Drzeniecka-Osiadacz, A., and Modzel, P.: Evaluation of low-cost sensors for ambient $\text{PM}_{2.5}$ monitoring, *J. Sensors*, 2018, 1–16, <https://doi.org/10.1155/2018/5096540>, 2018.
- Badura, M., Batog, P., Drzeniecka-Osiadacz, A., and Modzel, P.: Regression methods in the calibration of low-cost sensors for ambient particulate matter measurements, *SN Applied Sciences*, 1, 622, <https://doi.org/10.1007/s42452-019-0630-1>, 2019.
- Bezantakos, S., Schmidt-Ott, F., and Biskos, G.: Performance evaluation of the cost-effective and lightweight Alphasense optical particle counter for use onboard unmanned aerial vehicles, *Aerosol Sci. Tech.*, 52, 385–392, <https://doi.org/10.1080/02786826.2017.1412394>, 2018.
- Borghi, F., Spinazze, A., Campagnolo, D., Rovelli, S., Cattaneo, A., and Cavallo, D. M.: Precision and accuracy of a direct-reading

- miniaturized monitor in PM_{2.5} exposure assessment, *Sensors*, 18, 3089, <https://doi.org/10.3390/s18093089>, 2018.
- Bulot, F. M. J., Johnston, S. J., Basford, P. J., Easton, N. H. C., Apetroaie-Cristea, M., Foster, G. L., Morris, A. K. R., Cox, S. J., and Loxham, M.: Long-term field comparison of multiple low-cost particulate matter sensors in an outdoor urban environment, *Sci. Rep.-UK*, 9, 7497, <https://doi.org/10.1038/s41598-019-43716-3>, 2019.
- Cai, C., Stebounova, L. V., Peate, D. W., and Peters, T. M.: Evaluation of a Portable Aerosol Collector and Spectrometer to measure particle concentration by composition and size, *Aerosol Sci. Tech.*, 53, 675–687, <https://doi.org/10.1080/02786826.2019.1600654>, 2019.
- Castarède, D. and Thomson, E. S.: A thermodynamic description for the hygroscopic growth of atmospheric aerosol particles, *Atmos. Chem. Phys.*, 18, 14939–14948, <https://doi.org/10.5194/acp-18-14939-2018>, 2018.
- Cavaliere, A., Carotenuto, F., Di Gennaro, F., Gioli, B., Gualtieri, G., Martelli, F., Matese, A., Toscano, P., Vagnoli, C., and Zaldei, A.: Development of Low-Cost Air Quality Stations for Next Generation Monitoring Networks: Calibration and Validation of PM_{2.5} and PM₁₀ Sensors, *Sensors*, 18, 2843, <https://doi.org/10.3390/s18092843>, 2018.
- Chatzidiakou, L., Krause, A., Popoola, O. A. M., Di Antonio, A., Kellaway, M., Han, Y., Squires, F. A., Wang, T., Zhang, H., Wang, Q., Fan, Y., Chen, S., Hu, M., Quint, J. K., Barratt, B., Kelly, F. J., Zhu, T., and Jones, R. L.: Characterising low-cost sensors in highly portable platforms to quantify personal exposure in diverse environments, *Atmos. Meas. Tech.*, 12, 4643–4657, <https://doi.org/10.5194/amt-12-4643-2019>, 2019.
- Crilley, L. R., Shaw, M., Pound, R., Kramer, L. J., Price, R., Young, S., Lewis, A. C., and Pope, F. D.: Evaluation of a low-cost optical particle counter (Alphasense OPC-N2) for ambient air monitoring, *Atmos. Meas. Tech.*, 11, 709–720, <https://doi.org/10.5194/amt-11-709-2018>, 2018.
- Crilley, L. R., Singh, A., Kramer, L. J., Shaw, M. D., Alam, M. S., Apte, J. S., Bloss, W. J., Hildebrandt Ruiz, L., Fu, P., Fu, W., Gani, S., Gatari, M., Ilyinskaya, E., Lewis, A. C., Ng'ang'a, D., Sun, Y., Whitty, R. C. W., Yue, S., Young, S., and Pope, F. D.: Effect of aerosol composition on the performance of low-cost optical particle counter correction factors, *Atmos. Meas. Tech.*, 13, 1181–1193, <https://doi.org/10.5194/amt-13-1181-2020>, 2020.
- Di Antonio, A., Popoola, O. A. M., Ouyang, B., Saffell, J., and Jones, R. L.: Developing a relative humidity correction for low-cost sensors measuring ambient particulate matter, *Sensors*, 18, 2790, <https://doi.org/10.3390/s18092790>, 2018.
- Downward, G. S., van Nunen, E. J. H. M., Kerckhoffs, J., Vincis, P., Brunekreef, B., Boer, J. M. A., Messier, K. P., Roy, A., Verschuren, W. M. M., van der Schouw, Y. T., Sluijs, I., Gulliver, J., Hoek, G., and Vermeulen, R.: Long-term exposure to ultra-fine particles and incidence of cardiovascular and cerebrovascular disease in a prospective study of a Dutch cohort, *Environ. Health Persp.*, 126, 1–8, <https://doi.org/10.1289/EHP3047>, 2018.
- ECWG (European Commission Working Group): Guide to the demonstration of equivalence of ambient air monitoring methods, Report, Brussels, Belgium, 92 pp., 2010.
- Granados-Muñoz, M. J., Navas-Guzmán, F., Bravo-Aranda, J. A., Guerrero-Rascado, J. L., Lyamani, H., Valenzuela, A., Titos, G., Fernández-Gálvez, J., and Alados-Arboledas, L.: Hygroscopic growth of atmospheric aerosol particles based on active remote sensing and radiosounding measurements: selected cases in southeastern Spain, *Atmos. Meas. Tech.*, 8, 705–718, <https://doi.org/10.5194/amt-8-705-2015>, 2015.
- Hafkenscheid, T. L. and Vonk, J.: Evaluation of equivalence of the MetOne BAM-1020 for the measurement of PM_{2.5} in ambient air, RIVM Letter report 2014-0078), National Institute for Public Health and the Environment, Bilthoven, the Netherlands, 37 pp., 2014.
- Hagler, G. S. W., Williams, R., Papapostolou, V., and Polidori, A.: Air Quality Sensors and Data Adjustment Algorithms: When Is It No Longer a Measurement?, *Environ. Sci. Tech.*, 52, 5530–5531, <https://doi.org/10.1021/acs.est.8b01826>, 2018.
- Hänel, G.: The properties of atmospheric aerosol particles as functions of the relative humidity at thermodynamic equilibrium with the surrounding moist air, *Adv. Geophys.*, 19, 73–188, [https://doi.org/10.1016/S0065-2687\(08\)60142-9](https://doi.org/10.1016/S0065-2687(08)60142-9), 1976.
- Holstius, D. M., Pillarisetti, A., Smith, K. R., and Seto, E.: Field calibrations of a low-cost aerosol sensor at a regulatory monitoring site in California, *Atmos. Meas. Tech.*, 7, 1121–1131, <https://doi.org/10.5194/amt-7-1121-2014>, 2014.
- Jayaratne, R., Liu, X., Thai, P., Dunbabin, M., and Morawska, L.: The influence of humidity on the performance of a low-cost air particle mass sensor and the effect of atmospheric fog, *Atmos. Meas. Tech.*, 11, 4883–4890, <https://doi.org/10.5194/amt-11-4883-2018>, 2018.
- Karagulian, F., Barbieri, M., Kotsev, A., Spinelle, L., Gerboles, M., Lagler, F., Redon, N., Crunaire, S., and Borowiak, A.: Review of the Performance of Low-Cost Sensors for Air Quality Monitoring, *Atmosphere-Basel*, 10, 506, <https://doi.org/10.3390/atmos10090506>, 2019.
- Kelly, K. E., Whitaker, J., Petty, A., Widmer, C., Dybwad, A., Sleeth, D., Martin, R., and Butterfield, A.: Ambient and laboratory evaluation of a low-cost particulate matter sensor, *Environ. Pollut.*, 221, 491–500, <https://doi.org/10.1016/j.envpol.2016.12.039>, 2017.
- Kosmopoulos, G., Salamalikis, V., Pandis, S. N., Yannopoulos, P., Bloutsos, A. A., and Kazantzidis, A.: Low-cost sensors for measuring airborne particulate matter: Field evaluation and calibration at a South-Eastern European site, *Sci. Total Environ.*, 748, 141396, <https://doi.org/10.1016/j.scitotenv.2020.141396>, 2020.
- Kuula, J., Makela, T., Hillamo, R., and Timonen, H.: Response characterization of an inexpensive aerosol sensor, *Sensors*, 17, 2915, <https://doi.org/10.3390/s17122915>, 2017.
- Kuula, J., Mäkelä, T., Aurela, M., Teinilä, K., Varjonen, S., González, Ó., and Timonen, H.: Laboratory evaluation of particle-size selectivity of optical low-cost particulate matter sensors, *Atmos. Meas. Tech.*, 13, 2413–2423, <https://doi.org/10.5194/amt-13-2413-2020>, 2020.
- Li, H. Z., Gu, P., Ye, Q., Zimmerman, N., Robinson, E. S., Subramanian, R., Apte, J. S., Robinson, A. L., and Presto, A. A.: Spatially dense air pollutant sampling: Implications of spatial variability on the representativeness of stationary air pollutant monitors, *Atmos. Environ.*, 2, 1–13, <https://doi.org/10.1016/j.aaoa.2019.100012>, 2019.
- Magi, B. I., Cupini, C., Francis, J., Green, M., and Hauser, C.: Evaluation of PM_{2.5} measured in an urban setting using a low-cost optical particle counter and a Federal Equivalent Method

- Beta Attenuation Monitor, *Aerosol Sci. Tech.*, 54, 147–159, <https://doi.org/10.1080/02786826.2019.1619915>, 2020.
- Malings, C., Tanzer, R., Haurlyliuk, A., Saha, P. K., Robinson, A. L., Presto, A. A., and Subramanian, R.: Fine particle mass monitoring with low-cost sensors: Corrections and long-term performance evaluation, *Aerosol Sci. Tech.*, 54, 160–174, <https://doi.org/10.1080/02786826.2019.1623863>, 2020.
- Martin, R. V., Brauer, M., van Donkelaar, A., Shaddick, G., Narain, U., and Dey, S.: No one knows which city has the highest concentration of fine particulate matter, *Atmos. Environ.*, 3, 1–5, <https://doi.org/10.1016/j.aeaoa.2019.100040>, 2019.
- Masic, A., Bibic, D., Pikula, B., Dzaferovic-Masic, E., and Musemic, R.: Experimental study of temperature inversions above urban area using unmanned aerial vehicle, *Therm. Sci.*, 23, 3327–3338, <https://doi.org/10.2298/TSCI180227250M>, 2019.
- Masic, A., Bibic, D., Pikula, B., Blazevic, A., Huremovic, J., and Zero S.: Evaluation of optical particulate matter sensors under realistic conditions of strong and mild urban pollution, *Zenodo*, <https://doi.org/10.5281/zenodo.3897379>, 2020.
- Mie, G.: Beiträge zur Optik trüber Medien, speziell kolloidaler Metallösungen (contributions to the optics of diffuse media, especially colloid metal solutions, *Ann. Phys.*, 25, 377–445, <https://doi.org/10.1002/andp.19083300302>, 1908 (in German).
- Morawska, L., Thai, P. K., Liu, X., Asumadu-Sakyi, A., Ayoko, G., Bartonova, A., Bedini, A., Chai, F., Christensen, B., Dunbabin, M., Gao, J., Hagler, G. S. W., Jayaratne, R., Kumar, P., Lau, A. K. H., Louie, P. K. K., Mazaheri, M., Ning, Z., Motta, N., Mullins, B., Rahman, M. M., Ristovski, Z., Shafiei, M., Tjondronegoro, D., Westerdahl, D., and Williams, R.: Applications of low-cost sensing technologies for air quality monitoring and exposure assessment: How far have they gone?, *Environ. Int.*, 116, 286–299, <https://doi.org/10.1016/j.envint.2018.04.018>, 2018.
- Mukherjee, A., Stanton, L. G., Graham, A. R., and Roberts, P. T.: Assessing the utility of low-cost particulate matter sensors over a 12-week period in the Cuyama Valley of California, *Sensors*, 17, 1805, <https://doi.org/10.3390/s17081805>, 2017.
- Mukherjee, A., Brown, S. G., McCarthy, M. C., Pavlovic, N. R., Stanton, L. G., Snyder, J. L., D'Andrea, S., and Hafner, H. R.: Measuring Spatial and Temporal PM_{2.5} Variations in Sacramento, California, Communities Using a Network of Low-Cost Sensors, *Sensors*, 19, 4701, <https://doi.org/10.3390/s19214701>, 2019.
- Sayahi, T., Butterfield, A., and Kelly, K. E.: Long-term field evaluation of the Plantower PMS low-cost particulate matter sensors, *Environ. Poll.*, 245, 932–940, <https://doi.org/10.1016/j.envpol.2018.11.065>, 2019.
- Si, M., Xiong, Y., Du, S., and Du, K.: Evaluation and calibration of a low-cost particle sensor in ambient conditions using machine-learning methods, *Atmos. Meas. Tech.*, 13, 1693–1707, <https://doi.org/10.5194/amt-13-1693-2020>, 2020.
- Sousan, S., Koehler, K., Hallett, L., and Peters, T. M.: Evaluation of the Alphasense optical particle counter (OPC-N2) and the Grimm portable aerosol spectrometer (PAS-1.108), *Aerosol Sci. Tech.*, 50, 1352–1365, <https://doi.org/10.1080/02786826.2016.1232859>, 2016a.
- Sousan, S., Koehler, K., Thomas, G., Park, J. H., Hillman, M., Halterman, A., and Peters, T. M.: Inter-comparison of low-cost sensors for measuring the mass concentration of occupational aerosols, *Aerosol Sci. Tech.*, 50, 462–473, <https://doi.org/10.1080/02786826.2016.1162901>, 2016b.
- Sousan, S., Gray, A., Zuidema, C., Stebounova, L., Thomas, G., Koehler, K., and Peters, T.: Sensor selection to improve estimates of particulate matter concentration from a low-cost network, *Sensors*, 18, 3008, <https://doi.org/10.3390/s18093008>, 2018.
- Tanzer, R., Malings, C., Haurlyliuk, A., Subramanian, R., and Presto, A. A.: Demonstration of a low-cost multi-pollutant network to quantify intra-urban spatial variations in air pollutant source impacts and to evaluate environmental justice, *Int. J. Environ. Res. Public He.*, 16, 2523, <https://doi.org/10.3390/ijerph16142523>, 2019.
- Tasic, V., Jovasevic-Stojanovic, M., Vardoulakis, S., Milosevic, N. Kovacevic, R., and Petrovic, J.: Comparative assessment of a real-time particle monitor against the reference gravimetric method for PM₁₀ and PM_{2.5} in indoor air, *Atmos. Environ.*, 54, 358–364, <https://doi.org/10.1016/j.atmosenv.2012.02.030>, 2012.
- Tiszenkel, L., Stangl, C., Krasnomowitz, J., Ouyang, Q., Yu, H., Apsokardu, M. J., Johnston, M. V., and Lee, S.-H.: Temperature effects on sulfuric acid aerosol nucleation and growth: initial results from the TANGENT study, *Atmos. Chem. Phys.*, 19, 8915–8929, <https://doi.org/10.5194/acp-19-8915-2019>, 2019.
- Tryner, J., L'Orange, C., Mehaffy, J., Miller-Lionberg, D., Hofstetter, J. C., Wilson, A., and Volckens, J.: Laboratory evaluation of low-cost PurpleAir PM monitors and in-field correction using co-located portable filter samplers, *Atmos. Environ.*, 220, 117067, <https://doi.org/10.1016/j.atmosenv.2019.117067>, 2020.
- U.S. EPA: AirNow, available at: <https://www.airnow.gov/?city=Sarajevo&country=BIH>, last access: 26 November 2020.
- Walser, A., Sauer, D., Spanu, A., Gasteiger, J., and Weinzierl, B.: On the parametrization of optical particle counter response including instrument-induced broadening of size spectra and a self-consistent evaluation of calibration measurements, *Atmos. Meas. Tech.*, 10, 4341–4361, <https://doi.org/10.5194/amt-10-4341-2017>, 2017.
- Wang, Y., Li, J., Jing, H., Zhang, Q., Jiang, J., and Biswas, P.: Laboratory evaluation and calibration of three low-cost particle sensors for particulate matter measurement, *Aerosol Sci. Tech.*, 49, 1063–1077, <https://doi.org/10.1080/02786826.2015.1100710>, 2015.
- Zhang, J., Marto, J. P., and Schwab, J. J.: Exploring the applicability and limitations of selected optical scattering instruments for PM mass measurement, *Atmos. Meas. Tech.*, 11, 2995–3005, <https://doi.org/10.5194/amt-11-2995-2018>, 2018.
- Zhao, A., Bollasina, M. A., Crippa, M., and Stevenson, D. S.: Significant climate impacts of aerosol changes driven by growth in energy use and advances in emission control technology, *Atmos. Chem. Phys.*, 19, 14517–14533, <https://doi.org/10.5194/acp-19-14517-2019>, 2019.
- Zheng, T., Bergin, M. H., Johnson, K. K., Tripathi, S. N., Shirodkar, S., Landis, M. S., Sutaria, R., and Carlson, D. E.: Field evaluation of low-cost particulate matter sensors in high- and low-concentration environments, *Atmos. Meas. Tech.*, 11, 4823–4846, <https://doi.org/10.5194/amt-11-4823-2018>, 2018.
- Zheng, T., Bergin, M. H., Sutaria, R., Tripathi, S. N., Caldow, R., and Carlson, D. E.: Gaussian process regression model for dynamically calibrating and surveilling a wireless low-cost particulate matter sensor network in Delhi, *Atmos. Meas. Tech.*, 12, 5161–5181, <https://doi.org/10.5194/amt-12-5161-2019>, 2019.